Microfluid Nanofluid (2010) 8:423–443
DOI 10.1007/s10404-010-0580-9

REVIEW

Single-cell microfluidic impedance cytometry: a review

Tao Sun · Hywel Morgan

Received: 10 January 2010 / Accepted: 2 February 2010 / Published online: 6 March 2010

Abstract Lab-on-chip technologies are being developed for multiplexed single cell assays. Impedance offers a simple non-invasive method for counting, identifying and monitoring cellular function. A number of different microfluidic devices for single cell impedance have been developed. These have potential applications ranging from simple cell counting and label-free identification of different cell types or detecting changes in cell morphology after invasion by parasites. Devices have also been developed that trap single cells and continuously record impedance data. This technology has applications in basic research, diagnostics, or non-invasively probing cell function at the single-cell level. This review will describe the underlying principles of impedance analysis of particles. It then describes the state-of-the-art in the field of microfluidic impedance flow cytometry. Finally, future directions and challenges are discussed.

1 Introduction

Microfluidic single-cell analysis systems require technological solutions for counting, trapping, focusing, separating, sorting, characterisation and identification of single cells (Brown and Audet 2008; Chao and Ros 2008). Whilst bulk measurements on large populations of cells provide average information, individual cells, which are identical in appearance, generally have heterogeneous behaviour (Sims and Allbritton 2007; Svahn and Berg 2007). Therefore, high-throughput single-cell analysis methods are being developed that offer new approaches for characterising large numbers of single cells at high speed. Flow cytometry is a well-established technique for counting, identifying and sorting cells (Davey and Kell 1996; Shapiro 2004). Modern commercial fluorescence-activated-cell-sorting machines can analyse thousands of cells per second, but are generally expensive complex machines that are unsuited to handling small sample volumes. Lab-on-chip technologies (Manz et al. 1992; Whitesides and Stroock 2001; Thorsen et al. 2002; Beebe et al. 2002; Stone et al. 2004; Squires and Quake 2005; Whitesides 2006) offer new approaches for cell assays, and new technologies are being developed for high-speed cell manipulation.

Individual cells can be identified on the basis of differences in size and dielectric properties using electrical techniques which are non-invasive and label-free. Characterisation of the dielectric properties of biological cells is generally performed in two ways using AC electrokinetics or impedance spectroscopy. AC electrokinetic techniques are used to study the behaviour of particles (movement and/or rotation) and fluids subjected to an AC electric field. The electrical forces act on both the particles and the suspending fluid and have their origin in the charge and electric field distribution in the system. They are the basis of phenomena such as dielectrophoresis (Pohl 1978; Pethig 1979; Morgan and Green 2003; Voldman 2006; Sun et al. 2007a), travelling wave dielectrophoresis (Huang et al. 1993; Morgan et al. 1997), electrorotation (Arnold and Zimmermann 1988; Yang et al. 1999) and electroorientation (Jones 1995).

T. Sun (✉) · H. Morgan
Nano Research Group, School of Electronics and Computer Science, University of Southampton, Southampton SO17 1BJ, UK
e-mail: ts5@ecs.soton.ac.uk

H. Morgan
e-mail: hm@ecs.soton.ac.uk

Electrical impedance spectroscopy measures the AC electrical properties of particles (in suspension) from which the dielectric parameters of the particles can be obtained. The earliest work on bio-impedance measurements can be traced back to the 1910s (Höber 1910, 1912, 1913), where the low and high-frequency conductivity of erythrocytes was measured. This article was the first to estimate the conductivity of the interior of an erythrocyte. In 1924 and 1925, Fricke published a series of papers (Fricke 1924a, b, 1925a) that described the electrical conductivity and capacity of disperse systems using principles laid down by Maxwell (1873). Measurements of the capacitance of the suspending system (Fricke 1925b, c, d) were used to estimate the capacitance and thickness of the cell membrane at 8.1 mF m^{-2} and 3.3 nm, respectively, values that are remarkably close to the accepted values of today. Cole (1928a, b) used Maxwell's mixture equation to derive the complex impedance of a single-shelled cell in suspension. He proposed the Constant Phase Angle model (Cole 1932) to describe the behaviour of the cell membrane and derived the famous Cole–Cole plot. These authors published several papers (Cole 1935; Cole and Cole 1936a, b) on the electrical impedance of single oocytes. Single-cell measurements were firstly made in 1937 when Curtis and Cole (1937) using two electrodes embedded in a groove into which a single *Nitella* cell was placed. Schwan (1957, 1963) pioneered the field of cell impedance analysis, identifying three major dielectric dispersions (α, β and γ) for biological cells in suspension. The dispersion occurring at the lowest frequency termed the α-dispersion is attributed to polarisation of the double layer around the particle. Because this is found in the kHz frequency spectrum, it is difficult to measure because of electrical double layer (EDL) effects at the interface between the electrode and the electrolyte. The β-dispersion occurs in the MHz regime and originates from charging of the capacitive cell membrane. It is the most widely measured and used to determine cell membrane capacitance. In GHz range, dipolar relaxation of water gives the γ-dispersion. Schwan's contributions to the dielectric measurements of biological material have been summarised by Foster (2002).

This review summarises recent technological development in the field of microfluidic single-cell impedance analysis. We begin by introducing the Maxwell's mixture theory (Maxwell 1873) that describes the dielectric properties of single cells in suspension. Equivalent circuit models are presented to link the measured electrical properties with the dielectric properties of the system. We then review recent developments in single-cell microfluidic cytometry. Finally, we describe possible future developments and applications of the technology.

2 Theory

2.1 Maxwell's mixture theory

Impedance is the ratio of the voltage to current passing through the system. It is a measure of the dielectric properties (permittivity and conductivity) of the system. The dielectric behaviour of colloidal particles in suspension is generally described by Maxwell's mixture theory (Maxwell 1873). This relates the complex permittivity of the suspension to the complex permittivity of the particle, the suspending medium and the volume fraction. Based on Maxwell's mixture theory, shelled-models have been widely used to model the dielectric properties of particles in suspension (Hanai 1960; Pethig 1979; Wachner et al. 2002; Stewart et al. 2005; Asami 2002, 2006; Sun et al. 2007b, c) and are widely used to interpret experimental results in both AC electrokinetic and impedance measurements. For a cell in suspension, a single-shelled spherical model is normally used as shown in Fig. 1a.

The complex permittivity of the mixture is $\tilde{\varepsilon}_{\mathrm{mix}}$:

$$\tilde{\varepsilon}_{\mathrm{mix}} = \tilde{\varepsilon}_{\mathrm{m}} \frac{1 + 2\Phi\tilde{f}_{\mathrm{CM}}}{1 - \Phi\tilde{f}_{\mathrm{CM}}} \quad \text{with} \quad \tilde{f}_{\mathrm{CM}} = \frac{\tilde{\varepsilon}_{\mathrm{p}} - \tilde{\varepsilon}_{\mathrm{m}}}{\tilde{\varepsilon}_{\mathrm{p}} + 2\tilde{\varepsilon}_{\mathrm{m}}} \tag{1}$$

where $\tilde{\varepsilon} = \varepsilon - j\sigma/\omega$ is the complex permittivity, $j^2 = -1$, ω the angular frequency, $\tilde{f}_{\mathrm{CM}}$ is the Clausius–Mossotti and Φ is the volume fraction. The subscripts "p" and "m" refer to particle and medium, respectively.

The complex permittivity of the cell, $\tilde{\varepsilon}_{\mathrm{p}}$ is a function of the dielectric properties of membrane and cytoplasm, cell membrane $\tilde{\varepsilon}_{\mathrm{mem}}$ and internal properties $\tilde{\varepsilon}_{\mathrm{i}}$, and cell (inner radius R and membrane thickness d) given by:

$$\tilde{\varepsilon}_{\mathrm{p}} = \tilde{\varepsilon}_{\mathrm{mem}} \frac{\gamma^3 + 2\left(\frac{\tilde{\varepsilon}_{\mathrm{i}} - \tilde{\varepsilon}_{\mathrm{mem}}}{\tilde{\varepsilon}_{\mathrm{i}} + 2\tilde{\varepsilon}_{\mathrm{mem}}}\right)}{\gamma^3 - \left(\frac{\tilde{\varepsilon}_{\mathrm{i}} - \tilde{\varepsilon}_{\mathrm{mem}}}{\tilde{\varepsilon}_{\mathrm{i}} + 2\tilde{\varepsilon}_{\mathrm{mem}}}\right)} \quad \text{with} \quad \gamma = \frac{R + d}{R} \tag{2}$$

The Clausius–Mossotti factor $\tilde{f}_{\mathrm{CM}}$ characterises the frequency-dependent effective dipole moment. Separating the real and imaginary parts of the Clausius–Mossotti factor gives a Debye relaxation of the form:

$$\mathrm{Re}\left[\tilde{f}_{\mathrm{CM}}\right] = \left(\frac{\varepsilon_{\mathrm{p}} - \varepsilon_{\mathrm{m}}}{\varepsilon_{\mathrm{p}} + 2\varepsilon_{\mathrm{m}}}\right) + \frac{\left(\frac{\sigma_{\mathrm{p}} - \sigma_{\mathrm{m}}}{\sigma_{\mathrm{p}} + 2\sigma_{\mathrm{m}}}\right) - \left(\frac{\varepsilon_{\mathrm{p}} - \varepsilon_{\mathrm{m}}}{\varepsilon_{\mathrm{p}} + 2\varepsilon_{\mathrm{m}}}\right)}{1 + \omega^2\tau_{\mathrm{MW}}^2} \tag{3}$$

$$\mathrm{Im}\left[\tilde{f}_{\mathrm{CM}}\right] = \frac{\left[\left(\frac{\varepsilon_{\mathrm{p}} - \varepsilon_{\mathrm{m}}}{\varepsilon_{\mathrm{p}} + 2\varepsilon_{\mathrm{m}}}\right) - \left(\frac{\sigma_{\mathrm{p}} - \sigma_{\mathrm{m}}}{\sigma_{\mathrm{p}} + 2\sigma_{\mathrm{m}}}\right)\right]\omega\tau_{\mathrm{MW}}}{1 + \omega^2\tau_{\mathrm{MW}}^2} \tag{4}$$

with

$$\tau_{\mathrm{MW}} = \frac{\varepsilon_{\mathrm{p}} + 2\varepsilon_{\mathrm{m}}}{\sigma_{\mathrm{p}} + 2\sigma_{\mathrm{m}}} \tag{5}$$

where Re [ ] and Im [ ] are the real and imaginary parts, respectively. In AC electrokinetics (Morgan and Green

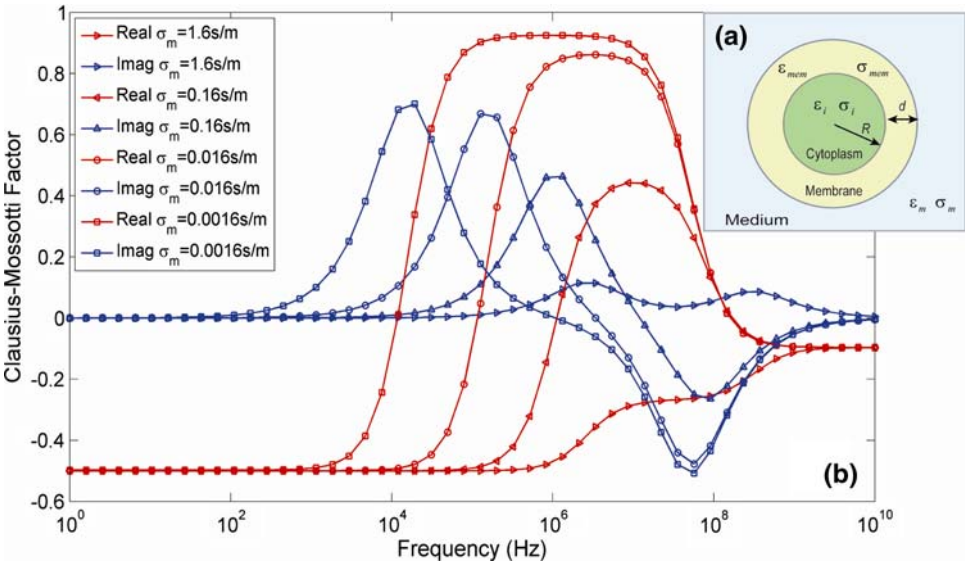

Fig. 1 **a** Diagram showing a single-shell spherical particle, representing a cell in suspension. **b** Plot showing a spectrum of the real and imaginary parts of the Clausius–Mossotti factor for a particle in an electrolyte, calculated for different suspending medium conductivities. The following parameters were used: $\varepsilon_o = 8.854 \times 10^{-12}$ F/m, $R = 3 \times 10^{-6}$ m, $d = 5 \times 10^{-9}$ m, $\varepsilon_m = 80 \times \varepsilon_o$, $\varepsilon_{mem} = 5 \times \varepsilon_o$, $\sigma_{mem} = 10^{-8}$ S/m, $\varepsilon_i = 60 \times \varepsilon_o$, $\sigma_i = 0.4$ S/m

2003), the frequency dependence and direction of the dielectrophoretic force are governed by the real part of the Clausius–Mossotti factor, whilst the electrorotation spectrum depends on the imaginary part of the Clausius–Mossotti factor. Figure 1b shows spectra of the real and imaginary parts of the Clausius–Mossotti factor of a cell for different suspending medium conductivities (see legends for details).

In Eq. 5, τ_{MW} is referred to as the Maxwell–Wagner relaxation time constant. For single cells in suspension, the suspending system has two intrinsic relaxation frequencies. The first relaxation (time constant τ_1) occurs at low frequencies and is due to (Maxwell–Wagner) polarisation of the cell membrane-suspending medium interface. The second relaxation (time constant τ_2) occurs at higher frequencies, and is due to polarisation between the suspending medium and the cell cytoplasm, when the cell membrane capacitance is effectively short-circuited. Figure 1b shows these two relaxations as the real and imaginary parts of the Clausius–Mossotti factor. For a cell, the real part of Clausius-Mossotti factor is negative at low frequencies, indicating that cell experiences negative dielectrophoresis (DEP) but at intermediate frequencies this varies with the conductivity of the suspending medium. Note that there are two electrorotational (ROT) peaks (imaginary part of Clausius–Mossotti factor), corresponding to τ_1 and τ_2. Characterisation of the dielectric properties of single cells is often performed by analysing the rotation spectra, in conjunction with measurements of the DEP cross-over frequency (Pohl 1978; Pethig 1979; Wang et al. 1993; Morgan and Green 2003).

Pauly and Schwan (1959) published a set of equations that describes the two characteristic relaxation time constants in terms of cell properties, specifically the cell membrane capacitance C_{mem} and cell membrane conductance G_{mem}:

$$\tau_1 = \mathrm{RC}_{\mathrm{mem}} \frac{\frac{1}{\sigma_i} + \left(\frac{1-\Phi}{2+\Phi}\right)\frac{1}{\sigma_m}}{1 + \mathrm{RG}_{\mathrm{mem}}\left[\frac{1}{\sigma_i} + \left(\frac{1-\Phi}{2+\Phi}\right)\frac{1}{\sigma_m}\right]} \tag{6a}$$

$$\tau_2 = \frac{\varepsilon_i + 2\varepsilon_m}{\sigma_i + 2\sigma_m} \tag{6b}$$

Their results are based on three approximations: (i) The conductivity of the cell membrane is considered very small compared with the cytoplasm and suspending medium conductivity ($\sigma_{mem} \ll \sigma_m$ and σ_i). (ii) The membrane thickness is small compared with the cell inner radius ($d \ll R$). (iii) The displacement current in the suspending medium and the cytoplasm is negligible compared with the conduction current ($\varepsilon_m = \varepsilon_i = 0$). Taken together, these three approximations make τ_1 independent of the permittivity of the suspending medium and cytoplasm, and τ_2 independent of the permittivity and conductivity of the membrane. Recently Laplace transform of Maxwell's mixture equation (Eqs. 1 and 2) was used to derive complete analytical expressions for the two characteristic relaxation time constants (Sun et al. 2007b).

Maxwell's mixture theory is only valid for dilute suspensions (volume fraction below 10%). For higher concentrations, interaction between the induced particles (dipoles) should be taken into account. Mixture theory was extended by Bruggeman (1935) and Hanai and colleagues (Hanai 1960; Hanai et al. 1975, 1979; Hanai and Koizumi 1976), to high volume fractions:

$$1 - \Phi = \left(\frac{\tilde{\varepsilon}_{mix} - \tilde{\varepsilon}_p}{\tilde{\varepsilon}_m - \tilde{\varepsilon}_p}\right)\left(\frac{\tilde{\varepsilon}_m}{\tilde{\varepsilon}_{mix}}\right)^{1/3} \tag{7}$$

The impedance of a system, e.g. cells in suspension, is related to the complex permittivity through

$$\tilde{Z}_{\text{mix}} = \frac{1}{j\omega\tilde{\varepsilon}_{\text{mix}} G_{\text{f}}} \tag{8}$$

where G_{f} is a geometric constant, which for an ideal parallel plate electrode system is simply the ratio of electrode area to gap A/g (m). This equation, together with Eq. 1, allows the complex permittivity of a suspension of cells to be determined from the frequency-dependent impedance measurements. Normally, a cell suspension is measured using planar or cylindrical electrode geometry where G_{f} can be easily defined. However, for single-cell impedance analysis, the cell is located in an electric field generated by two micro-electrodes. In this case, the field is not uniform and the effect of the divergent field (fringing field) must be considered to correctly model the impedance. This involves detailed analysis of the field geometry and a modification to G_{f}—see later.

2.2 Equivalent circuit model

For simplified analysis of the system, an electrical circuit analogue is often used and such an approach was developed by Foster and Schwan (1989). The cell is approximated to a resistor that describes the cytoplasm in series with a capacitor for the membrane as shown in Fig. 2a. The cell membrane resistance is generally much greater than the reactance of the membrane and is ignored. Likewise, the capacitance of the cell cytoplasm can be ignored when its reactance is compared to the cell cytoplasm resistance. The values of the electrical components in the circuit are as follows:

Suspending medium:

$$R_{\text{m}} = \frac{1}{\sigma_{\text{m}}(1 - 3\Phi/2) G_{\text{f}}} \tag{9a}$$

$$C_{\text{m}} = \varepsilon_{\infty} G_{\text{f}} \tag{9b}$$

Simplified cell components:

$$C_{\text{mem}} = \frac{9\Phi \text{RC}_{\text{mem},0}}{4} G_{\text{f}} \tag{9c}$$

$$R_{\text{i}} = \frac{4\left(\frac{1}{2\sigma_{\text{m}}} + \frac{1}{\sigma_{\text{i}}}\right)}{9\Phi G_{\text{f}}} \tag{9d}$$

with specific membrane capacitance (per unit area) $C_{\text{mem},0} = \varepsilon_{\text{mem}}/d$. The limiting high-frequency permittivity of the suspension is related to the suspending medium permittivity according to

$$\varepsilon_{\infty} \simeq \varepsilon_{\text{m}}\left[1 - 3\Phi \frac{\varepsilon_{\text{m}} - \varepsilon_{\text{i}}}{2\varepsilon_{\text{m}} + \varepsilon_{\text{i}}}\right] \tag{9e}$$

Foster and Schwan's simplified circuit model has been used to interpret single-cell impedance measurements (Gawad et al. 2001, 2004; Morgan et al. 2007; Sun et al. 2007c, d) providing good agreement with experiments.

In certain cases, the cell membrane conductance and cytoplasm capacitance cannot be ignored, for example during electroporation (Tsong 1991) or cell lysis (Lu et al. 2005), where the resistance of the cell membrane and the capacitance of the cytoplasm vary widely. In this case, a complete equivalent circuit model is required. For a single-shelled spherical particle, this will include the resistance of the membrane and the capacitance of the cytoplasm (Sun et al. 2009a). The complete circuit model is shown in Fig. 2b, and the values of the electrical components are

Suspending medium:

$$R'_{\text{m}} = \frac{1}{\sigma_0 G_{\text{f}}} \tag{10a}$$

$$C'_{\text{m}} = \varepsilon'_{\infty} G_{\text{f}} \tag{10b}$$

Complete cell components:

$$R'_{\text{mem}} = \frac{1}{G_{\text{f}}}\left[\frac{\tau_1 + \tau_2}{\Delta\varepsilon_1 + \Delta\varepsilon_2} - \frac{1}{k_2 + k_3} - \frac{\tau_1\tau_2(k_2 + k_3)}{(\Delta\varepsilon_1 + \Delta\varepsilon_2)^2}\right] \tag{11a}$$

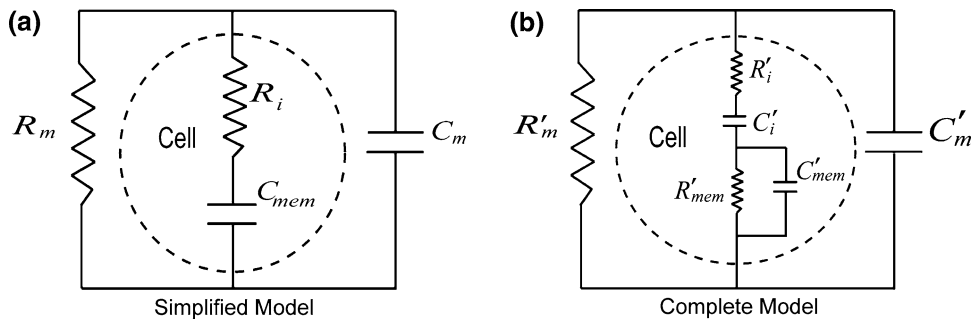

Fig. 2 **a** Foster and Schwan's simplified circuit model for a single-cell in suspension. The cell is modelled as a resistor R_{i} (cytoplasm) and a capacitor C_{mem} (membrane) in series. **b** The complete circuit model for a single-shelled particle in suspension. The particle is modelled as a resistor R'_{i} and a capacitor C'_{i} in series (cytoplasm) in combination with a resistor R'_{mem} and a capacitor C'_{mem} in parallel (membrane)

$$C'_{\text{mem}} = \frac{\tau_1\tau_2(k_2+k_3)}{(\Delta\varepsilon_1+\Delta\varepsilon_2)R'_{\text{mem}}} \tag{11b}$$

$$R'_{\text{i}} = \frac{1}{(k_2+k_3)G_{\text{f}}} \tag{11c}$$

$$C'_{\text{i}} = (\Delta\varepsilon_1+\Delta\varepsilon_2)G_{\text{f}} \tag{11d}$$

where R'_{mem} and C'_{mem} are the resistance and capacitance of the cell membrane, respectively. R'_{i} and C'_{i} are the resistance and capacitance of the inner core (cell cytoplasm), respectively. Full details of these equations can be found in the study of Sun et al. (2007b, 2009a).

3 Coulter counter

The first cytometer capable of measuring the electrical properties of single particles was developed by Coulter (1956). The device measures the DC resistance between two electrically isolated fluid-filled chambers and the change in this as particles pass through a small connecting orifice (Fig. 3). Two large electrodes are positioned at either side of an orifice. As a particle passes through the orifice, it displaces the conductive fluid and alters the resistance, this change is measured as a current pulse. Each pulse corresponds to the movement of a single particle and the magnitude is proportional to the amount of fluid displaced, i.e. cell size. A simplified analysis of the Coulter counter was given by Deblois and Bean (1970). The resistance of a tube, diameter D_{t}, length L_{t}, filled with electrolyte of resistivity ρ_{m} (Fig. 3) is

$$R_{\text{t}} = \frac{4\rho_{\text{m}}L_{\text{t}}}{\pi D_{\text{t}}^2} \tag{12}$$

Deblois and Bean (1970) used Maxwell's approximation to evaluate the resistance of the tube containing a spherical particle (diameter d_{p}). Here, we show how Maxwell's approximation is a simplified form of Maxwell's mixture theory. Considering only the conductivity component in Eq. 1, the conductivity of the mixture can be written as

$$\begin{aligned}\sigma_{\text{mix}} &= \sigma_{\text{m}}\frac{1+2\Phi\left(\frac{\sigma_{\text{p}}-\sigma_{\text{m}}}{\sigma_{\text{p}}+2\sigma_{\text{m}}}\right)}{1-\Phi\left(\frac{\sigma_{\text{p}}-\sigma_{\text{m}}}{\sigma_{\text{p}}+2\sigma_{\text{m}}}\right)} \\ &= \sigma_{\text{m}}\left[1+3\Phi\frac{\sigma_{\text{p}}-\sigma_{\text{m}}}{(1-\Phi)\sigma_{\text{p}}+(2+\Phi)\sigma_{\text{m}}}\right]\end{aligned} \tag{13}$$

For low volume fraction ($\Phi \ll 1$), Eq. 13 can be approximated to

$$\sigma_{\text{mix}} \simeq \sigma_{\text{m}}\left(1+3\Phi\frac{\sigma_{\text{p}}-\sigma_{\text{m}}}{\sigma_{\text{p}}+2\sigma_{\text{m}}}\right) \tag{14}$$

and written in terms of resistivity, Maxwell's approximation is

$$\begin{aligned}\rho_{\text{mix}} &= \rho_{\text{m}}\left[1+3\Phi\frac{\rho_{\text{p}}-\rho_{\text{m}}}{(2\rho_{\text{p}}+\rho_{\text{m}})+3\Phi(\rho_{\text{m}}-\rho_{\text{p}})}\right] \\ &\simeq \rho_{\text{m}}\left(1+3\Phi\frac{\rho_{\text{p}}-\rho_{\text{m}}}{2\rho_{\text{p}}+\rho_{\text{m}}}\right) \\ &= \rho_{\text{m}}\left[1+\frac{3\Phi}{2}+\left(\frac{-9\Phi\rho_{\text{m}}}{4\rho_{\text{p}}+2\rho_{\text{m}}}\right)\right]\end{aligned} \tag{15a}$$

For an insulating particle (i.e. a cell measured at low frequencies) this becomes

$$\rho_{\text{mix}} \simeq \rho_{\text{m}}\left(1+\frac{3\Phi}{2}\right) \tag{15b}$$

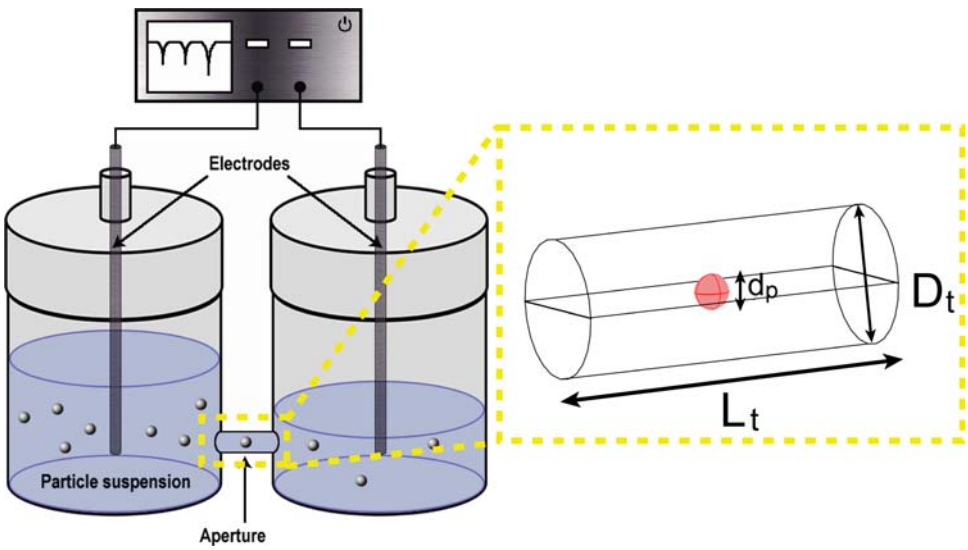

Fig. 3 Illustrating the working principles of the Coulter counter. A suspension of particles or biological cells flow through a sensing aperture through which current flows. The current is modulated (reduced) as a particle passes through, so that individual cells can be counted and sized

The volume fraction of a particle in a tube is

$$\Phi = \frac{2d_p^3}{3D_t^2 L_t} \tag{16}$$

Combining Eqs. 12, 15 and 16, the resistance of the mixture is

$$R_{mix} = \frac{4\rho_{mix}L_t}{\pi D_t^2} = \frac{4\rho_m L_t}{\pi D_t^2}\left(1 + \frac{d_p^3}{D_t^2 L_t}\right) \tag{17}$$

as in Deblois and Bean (1970). The resistance change ΔR due to the particle is given by

$$\Delta R = R_{mix} - R_t = \frac{4\rho_m d_p^3}{\pi D_t^4} \tag{18}$$

Equation 18 is based on the assumption that the particle diameter is small compared with the tube ($\Phi \ll 1$), but ignores other issues such as access resistance to the tube. Deblois and Bean (1970) gave a solution applicable over a broader range:

$$\Delta R_{(D_t/L_t \ll 1)} = \left(\frac{4\rho_m d_p^3}{\pi D_t^4}\right) \cdot F\left(\frac{d_p^3}{D_t^3}\right) \tag{19}$$

where $F\left(d_p^3 \Big/ D_t^3\right)$ is a correction term that accounts for the non-uniformity of the current density within the tube.

According to Eq. 18, the sensitivity of the Coulter counter depends on the fourth power of the orifice diameter. A small orifice is used to detect small particles, but restricts the overall range of particle sizes that can be measured. To increase the sensitivity, the current flux through the orifice must be increased. Usually a large orifice is used together with a low conductivity sheath fluid (Spielman and Gorsen 1968; Shuler et al. 1972). A limitation of the Coulter counter is that DC resistance measurements only provide size information. Hoffman et al. (1979, 1981) developed a flow-system, based on the Coulter counter design, where an AC current flows through the orifice to measure the impedance of cells at higher frequencies. This article was the first demonstration of a device for high-speed single-cell impedance analysis. The simplicity and sensitivity of the Coulter technique contributed to its rapid development and commercialisation (i.e. Beckman Coulter, Fullerton, CA, USA) and is a classical example of resistive-pulse sensor (Bayley and Martin 2000).

The earliest design of a micro-fabricated Coulter counter consisted of an aperture fabricated in silicon with a glass cover (Larsen et al. 1997). A four-point electrode arrangement was integrated on the bottom of the channel; however, no data were published. Koch et al. (1999) also fabricated a micro-Coulter counter using an etched silicon trench with metal electrodes. Again, no experimental data were reported. Saleh and Sohn (2001) fabricated a micro-Coulter counter on a quartz substrate with pore dimension of 5.1 × 1.5 × 1.0 μm^3 (Fig. 4a). They measured colloids ranging from 190 to 640 nm in diameter and obtained a resolution of ±10 nm in diameter (Fig. 4b). Satake et al. (2002) developed a silicon-based Coulter counter and counted polystyrene beads and red blood cells (RBCs). Experiments showed good linearity between the number of recorded pulses and the concentration of particles. In 2003, Saleh and Sohn (2003a, b) further extended the technology to measure nanoparticles. They fabricated a polydimethylsiloxane (PDMS) channel with a 200 nm constriction and detected single DNA molecules and antibody binding onto nano-beads. The concept of a micro-Coulter counter for analysing nano-particles has evolved into sophisticated nanopore devices capable of single molecule analysis and high-throughput sequencing single-stranded genomic DNA or RNA (see Branton et al. 2008 for an overview).

In recent years, several groups have endeavoured to improve on the micro-Coulter counter, addressing issues such as channel clogging, throughput, and sensitivity. Nieuwenhuis et al. (2004) used a 'liquid aperture' to overcome channel clogging. The aperture was defined using a non-coaxial sheath of conductive sample fluid,

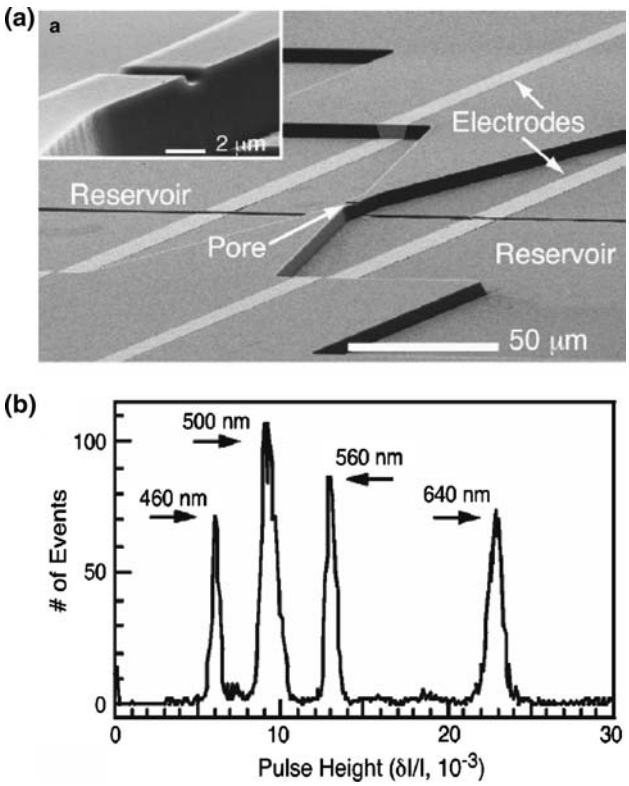

Fig. 4 **a** Scanning electron micrograph of a micro-Coulter counter. **b** A histogram of pulse heights, demonstrating a resolution of ±10 nm in particle diameter (adapted with permission from Saleh and Sohn 2001, copyright© 2001, American Institute of Physics)

surrounded on three sides by a non-conductive sheath liquid. As shown in Fig. 5a, the vertical dimensions of the Coulter aperture are controlled by the relative flowrate between the sample solution and sheath flow. The relatively high sheath flowrate reduces the height of the aperture. The horizontal dimensions of the Coulter aperture are controlled by two control ports on the sides of the channel. Since the physical dimensions of the channel are much larger than the Coulter aperture, this use of hydrodynamic focussing prevents channel blocking. In Fig. 5b, the sample solution (red in online color version) demonstrates a stable sheath flow and the Coulter aperture can be controlled over a large range.

Throughput can be improved using multi-aperture designs (Jagtiani et al. 2006a, b) or multiple-channels (Zhe et al. 2007). Jagtiani et al. (2006a, b) designed a four-aperture (Fig. 6a) Coulter counter to measure particles flowing through four channels simultaneously. Each sub-Coulter counter had its own interrogation electrodes and electronics. Zhe et al. (2007) designed a four-channel parallel micro-Coulter counter sharing a single sample reservoir (Fig. 6b). The device has a common electrode and four central electrodes for each channel. A constant DC supply was connected to the common electrode at one end and to a sampling resistor at the other end. The device detects particles flowing through the four sensing channels simultaneously and thus enables higher throughput.

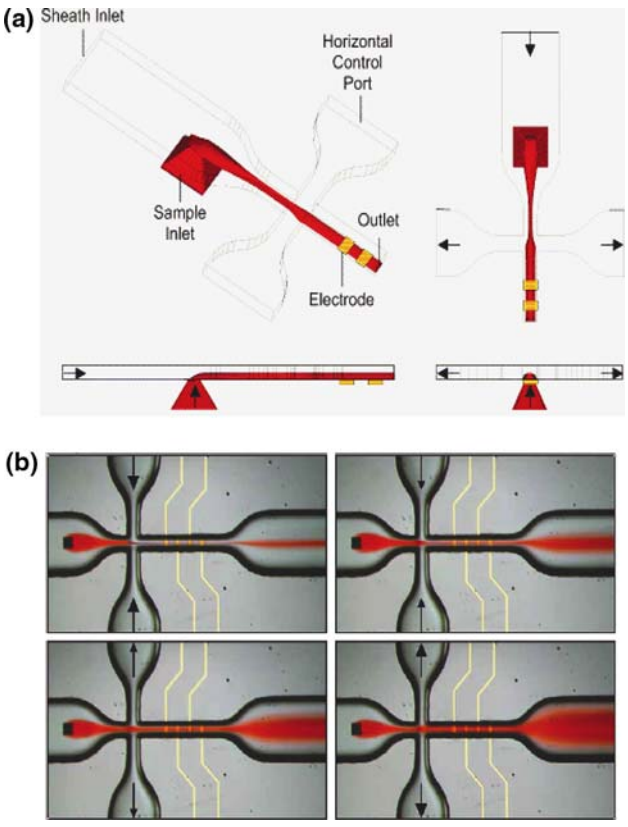

Fig. 5 **a** The Coulter aperture can be controlled in two dimensions by varying the relative flow-rates at the sample inlet and control inlets. **b** Experimental results using a dye (red in online color version) for sample solution, demonstrating stable sheath flow in the channel, and how the aperture size can be varied (adapted with permission from Nieuwenhuis et al. 2004, copyright© 2004, Elsevier)

Most Coulter designs measure particle properties at low frequencies using non-polarisable electrodes like Ag/AgCl but these electrodes are unsuitable for high frequency measurements and they also have a limited lifetime. For wide-band impedance measurements, metal electrodes are used. Unfortunately the formation of an EDL at the interface between the electrode and the suspending medium (Schwan 1968; Bard and Faulkner 2000) causes other problems. The EDL can be thought of as a capacitor which is in series with the sample; at low frequencies the impedance of the EDL capacitor dominates the system so that only a small fraction of the voltage appears in the sample. One solution to minimise this EDL effect is to increase the surface area of the electrodes. Zheng et al. (2008) fabricated a miniature Coulter device with electroplated platinum-black electrodes. The surface roughness of electrodes increased from 6.75 to 238 nm after electroplating. The authors demonstrated an improvement in the low-frequency performance and were able to size polystyrene beads and human RBCs at a frequency of 10 kHz.

Several papers have demonstrated microfabricated microfluidic sensors for single particle counting (Tang and Gao 2005; Chun et al. 2005; Cho et al. 2006; Wu et al. 2008a, b; Kim et al. 2009) and a recent review on microfluidic systems for counting particles using electrical and optical methods has been published (Zhang et al. 2009). One issue with Coulter counters is detecting small particles in a large aperture. Wu et al. (2008a) used a two-stage differential amplification scheme in a symmetric mirror-channel structure to increase the signal-to-noise ratio (SNR). Particles were detected at a volume fraction in the sensing aperture of 0.0004%, equivalent to a particle size of 520 nm in diameter in a sensing aperture of $50 \times 16 \times 20\ \mu m^3$. Further designs had integrated fluorescent detectors (Wu et al. 2008b) for simultaneous electrical and optical detection of single particles. A velocimetry chip (Chun et al. 2005) utilised a polyelectrolyte salt bridge-based electrode (PSBE). The PSBEs were fabricated using a photopolymerisation technique and as shown in Fig. 7a, were connected to an impedance analyser through isotonic NaCl solutions and Ag/AgCl electrodes, respectively. Figure 7b shows the use of the device for counting RBCs and white blood cells (WBCs) in human blood. The size difference between RBCs and WBCs can be clearly resolved. The throughput of the device is claimed to be 1000 cells/s, which the authors attribute to

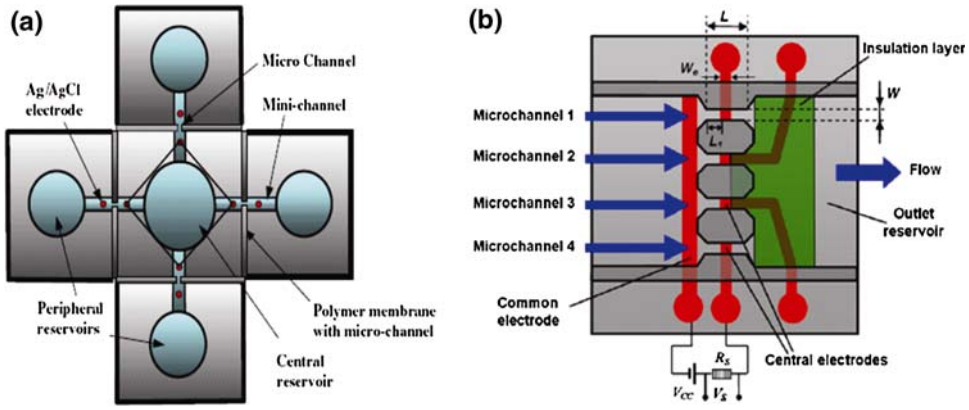

Fig. 6 **a** A high-throughput resistive-pulse sensor consisting of four peripheral reservoirs and a main central reservoir (adapted with permission from Jagtiani et al. 2006a, b, copyright© 2006, IOP). **b** A schematic diagram of a four-channel Coulter counter (adapted with permission from Zhe et al. 2007, copyright© 2007, IOP)

the quick response of the analysis system which can only be done with PSBEs, because metal electrodes have an EDL and/or Faradaic reactions on the surfaces. The lifetime of the non-polarisable Ag/AgCl electrodes is a limiting factor in the design and a typical 1 h running time was reported by the authors. Recently, a similar design (Kim et al. 2009) used polyelectrolyte gel electrodes for counting RBCs.

4 Microfluidic impedance cytometry

4.1 Impedance analysis of flowing cells

Impedance micro-cytometry is an evolution of the micro-Coulter counter, but instead of fabricating an aperture with sensing electrodes either side, microelectrodes are integrated into the walls of the microchannel. Ayliffe et al. (1999) was the first to demonstrate single-cell impedance measurements in a micro-device. They fabricated a microchannel (10 μm wide and 4.3 μm high) from epoxy-based photoresist on glass substrate with integrated gold electrodes (8 μm wide and 4 μm thick), as shown in Fig. 8a. Impedance spectra over a frequency range from 100 kHz to 2 MHz were measured for human polymorphonuclear leukocytes (PMNs) and fish RBCs suspended in different concentrations of phosphate buffered saline (see Fig. 8b). This device shown was able to differentiate between cells and demonstrated the potential of single-cell impedance analysis.

Impedance measurements at multiple frequencies (within a bandwidth of 10 MHz) were performed by Fuller et al. (2000), who characterised human peripheral blood granulocytes, and measured radius, membrane capacitance and cytoplasm conductivity. The throughput of the device was up to 100 particles/s. Sohn et al. (2000) developed "capacitance cytometry" and claimed to measure the DNA content of fixed eukaryotic cells. A PDMS microchannel was fabricated over a pair of gold electrodes. Distinct peaks, representing the electrical properties of individual cells, were measured using a capacitance bridge at a frequency of 1 kHz which measures cell size, like a Coulter counter. Results showed a linear relationship between the capacitance and the DNA content of a cell, probably reflecting change in cell volume.

A significant advance in single-cell impedance technology was reported by Gawad et al. (2001), who demonstrated clear differentiation of beads and also erythrocytes and ghost cells. The principle of single-cell impedance analysis using this approach is shown in Fig. 9a. Two pairs of microelectrodes are fabricated on the bottom of a microchannel. The electrodes are energised with a voltage at one or more discrete frequencies,

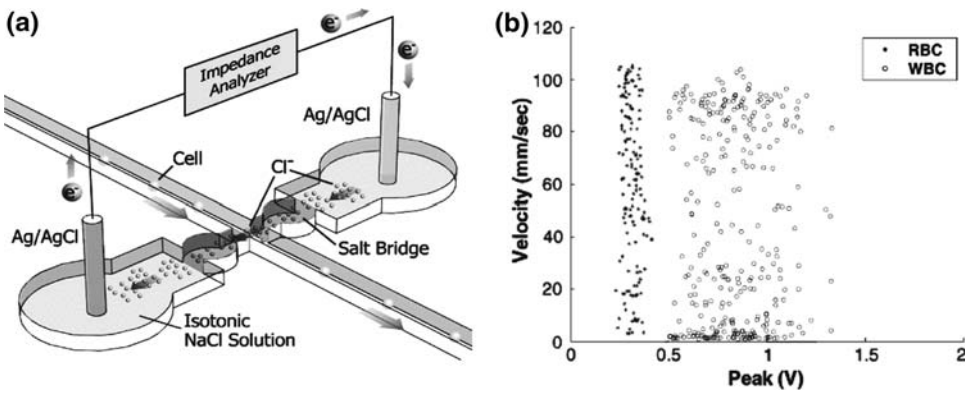

Fig. 7 **a** A micro-Coulter system where the DC resistance is measured across the channel. A bias of 0.4 V is applied between two Ag/AgCl electrodes, electrochemically connected to two PSBE through a NaCl solution. **b** Scatter plot of the velocity and peak amplitude for RBCs and WBCs flowing through the velocimetry chip (adapted with permission from Chun et al. 2005, copyright© 2005, ACS)

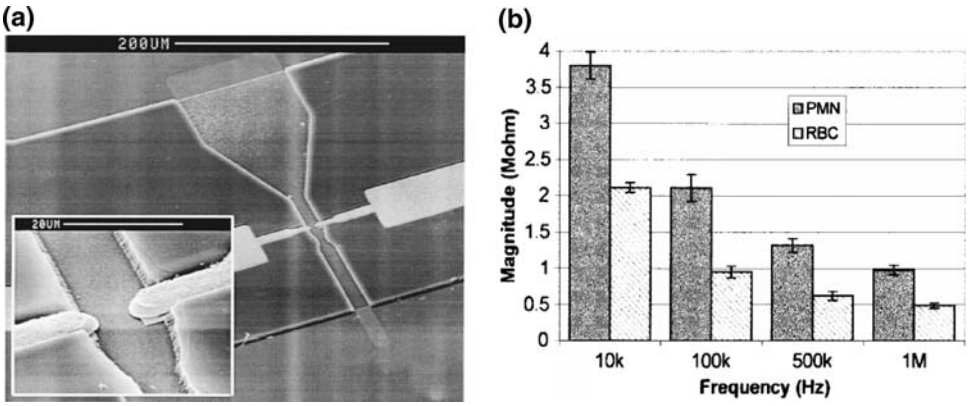

Fig. 8 **a** SEM of a microchannel with integrated gold electrodes that was used for single-cell impedance measurements. **b** Impedance magnitude data for human PMNs and fish RBCs at four different frequencies showing that the differences in cell types could be identified (adapted from Ayliffe et al. 1999, copyright© 1999, IEEE)

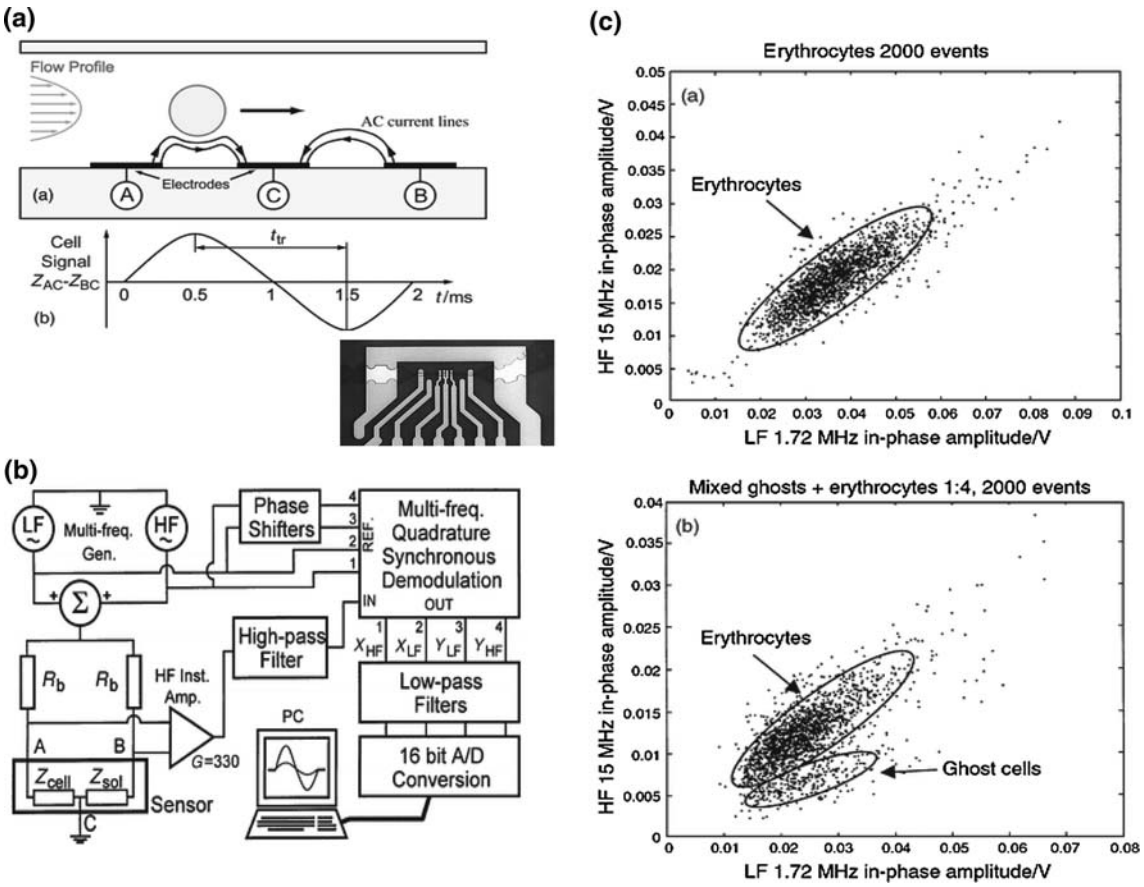

Fig. 9 **a** Schematic diagram showing a particle flowing over a three-electrode micro-impedance chip, and a typical impedance signal for a single particle. The image (*right hand corner*) shows the microelectrodes within the channel. **b** The electronic sub-components showing the excitation, amplification and demodulation parts of the mixed-frequency detection circuit. **c** Impedance scatter plots for particles flowing through the device. *Upper figure* shows the in-phase component of the impedance signal for 2,000 erythrocytes plotted for two different frequencies. *Lower image* is data for ghost cells and erythrocytes at a 1:4 ratio. From the impedance data the cell size is estimated (adapted with permission from Gawad et al. 2001, copyright© 2001, RSC)

generating a non-uniform electric field within the channel. One pair is used for sensing the electric current fluctuation caused by a cell, whereas the other measures the electric current passing through the pure medium and acts as a reference. To detect the impedance signal from a single cell, microelectrodes are fabricated with sizes similar to a cell, in the range 10–30 μm. The electrical current from two sensing volumes is converted into voltage signals using trans-impedance amplifiers. Then, a differential amplifier subtracts the difference between the two signals. Lock-in amplifiers are used to demodulate the in-phase and out-phase impedance signals at the stimulating frequency,

whilst rejecting noise at other frequencies (Fig. 9b). The differential variation in impedance is measured as a pair of peaks. This differential impedance sensing scheme provides several advantages (Gawad et al. 2001): (i) the properties of the cell is measured directly against the suspending medium; (ii) any uneven drift in the properties of the electrodes is cancelled; (iii) the velocity of the flowing cells is determined from the transit time between the peaks. Figure 9c shows impedance data (scatter plot) for erythrocytes and a mixture of erythrocytes and ghost cells. This article was the first demonstration of quantitative analysis demonstrating discrimination of two cell populations.

The coplanar electrodes design (Fig. 9a) proposed by Gawad et al. (2001) was adapted for single particle/cell impedance sensing and counting by many authors (Nieuwenhuis et al. 2004; Wood et al. 2005, 2007a, b; Morgan et al. 2006; Benazzi et al. 2007; Küttel et al. 2007; Iliescu et al. 2007; Rodriguez-Trujillo et al. 2007, 2008; Murali et al. 2009). High-speed measurements were demonstrated by Wood et al. (2005) who used a radio frequency resonance detection technique with coplanar electrodes to eliminate stray capacitance effect at high frequencies and particles could be counted at a throughput of 25000/s. However, the amplitude of the detected peaks, which is a measure of particle size, varies widely, so that accurate sizing is not possible at such a high flowrate.

The non-homogeneous electric field distribution caused by planar microelectrodes has a major influence on the variation in the impedance signal amplitude. This is because nominally identical particles flowing at different positions in the channel experience different electric field strength and generate a different impedance signal. Accurate mapping of the electric field distribution within the microchannel is required to model the impedance spectrum of a single cell. Gawad et al. (2004) performed 3D finite-element modelling of a pair of parallel facing electrodes (Fig. 10a) to calculate the electric field and compared numerical solutions with Maxwell's mixture equation (Fig. 10b). Linderholm et al. (2005, 2006) and Sun et al. (2007c) used conformal mapping method to analytically solve the electric field distribution for both a coplanar and parallel facing electrode design. It was demonstrated that the control of particle position is more significant for the coplanar design than for the parallel electrode configuration because the electric field distribution in the latter design is least divergent (Sun et al. 2007c).

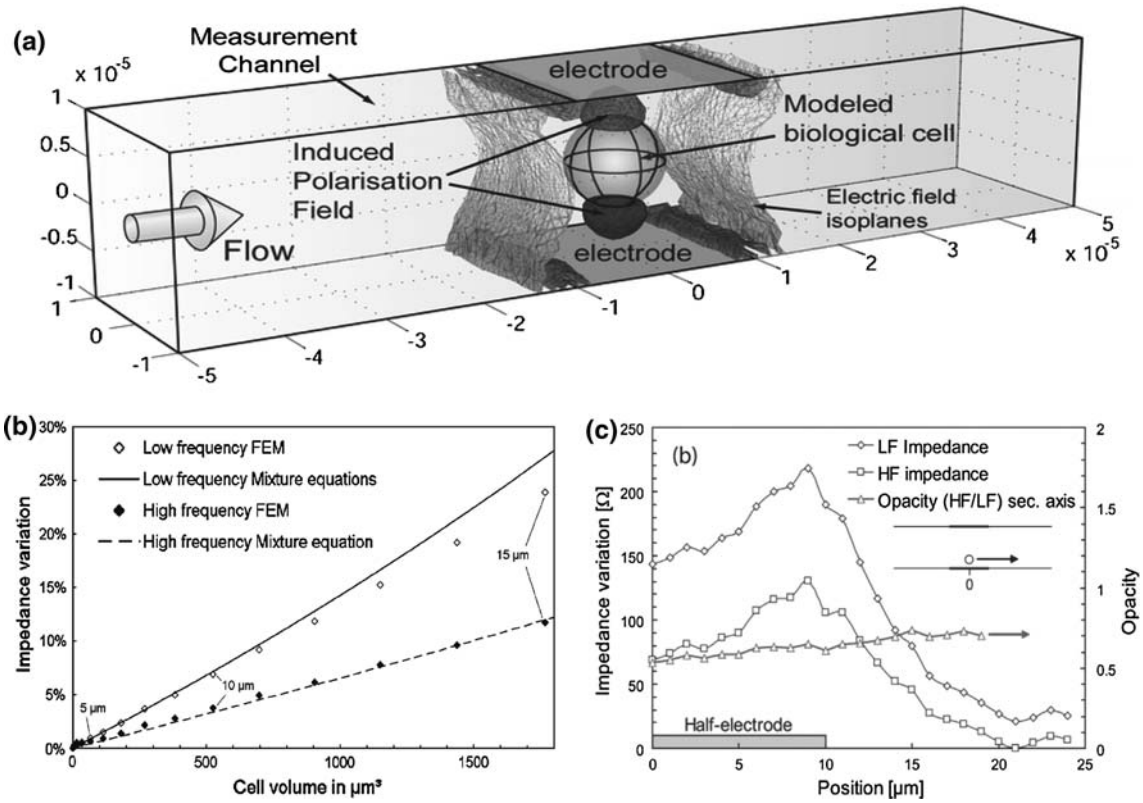

Fig. 10 **a** A cell between two microelectrodes in a microfluidic channel and the electric field. **b** Plots comparing finite-element modelling (*dots*) and Maxwell's mixture equation (*lines*), of the impedance change for different cell sizes. **c** The change in impedance (at two different frequencies) for a 4-µm diameter cell moving along a trajectory 7 µm below the centre line of the channel. The opacity calculation demonstrates much lower sensitivity to position that the low or high frequency impedance (adapted with permission from Gawad et al. 2004, copyright© 2004, RSC)

The geometric G_f constant in Eq. 8 relates the measured impedance to the system complex permittivity. To account for the non-homogeneity of the electric field distribution in the cytometer, values of G_f have been published (Gawad et al. 2004). This geometric factor depends on the length of the electrode, width and height of the channel and full derivations of this geometric factor for both coplanar and parallel facing electrodes designs have been derived in Sun et al. (2007c).

Plotting the ratio of the high-to-low-frequency impedance data, termed 'opacity', normalises the cell properties for size and also for position in the channel (Gawad et al. 2004). This effect is illustrated in Fig. 10c, where the magnitude of the impedance (calculated numerically) for high and low frequencies is plotted as a function of the position of a cell along the electrodes. It can be seen that although the impedance signal changes, the opacity is much less influenced by position.

Cheung et al. (2005) used a chip with parallel facing electrodes to measure the dielectric properties of RBCs. They compared the difference between ghosts and RBCs where the membrane proteins had been fixed using glutaraldehyde. They showed that the opacity of RBCs with fixed cell membranes was significantly different from normal RBCs. A similar system was used by Kampmann et al. (2008) to discriminate various cell types.

Figure 11a shows a photograph of the type of chip used for these experiments, with channel dimensions in the range 20–30 μm. Figure 11b shows a simulated plot showing the variation in magnitude and phase of the impedance with frequency for a "typical" cell, based on the equivalent circuit model (Eq. 9) through PSpice. It shows that the low-frequency behaviour is dominated by the EDL, and that at around 500 kHz cells can be accurately sized. At intermediate frequencies, the membrane capacitance dominates behaviour, whereas at high frequencies, the cell cytoplasm becomes important. An example of the use of high frequency measurements for cell analysis was reported by Küttel et al. (2007), who detected infection of RBCs with the parasite *Babesia bovis* using a signal at 8.7 MHz and low conductivity suspending media. The reduction in conductivity reduces the characteristic membrane charging frequency—Eq. 6a and reduces the frequency required to probe intracellular properties. Theses authors demonstrated differentiation of parasitised RBCs from uninfected RBCs and ghost RBCs due to the changes in the electrical properties of the cell cytoplasm.

Extending the frequency range of impedance measurements will further aid in interrogating intracellular properties. Very recently, Ferrier et al. (2009) reported a microwave interferometric system, made from a resonant transmission line for detecting capacitance changes from a single cell at a frequency of 1.6 GHz. Preliminary experimental results showed time-dependent capacitance changes as yeast cells flowed over the interdigitated electrode array.

Single-cell impedance analysis in micro-cytometry is performed at high speed, usually with two excitation signals as shown in Fig. 9b. Measurement of the frequency spectrum for a single-cell population can be performed by sweeping a stimulation signal over a range of frequencies whilst cells flow through the device (Gawad et al. 2001, 2004; Cheung et al. 2005; Morgan et al. 2006, Holmes et al. 2009). The disadvantage of this approach is that although single cells are measured, the data represent the average for the population and are not a true measurement of an individual cell. A high-speed multi-frequency analysis system to characterise single particles was developed by Fuller et al. (2000), using multiple fixed frequencies demodulated with lock-in systems. However, the system is complicated and requires a large amount of mixed-signal hardware. Sun et al. (2007d, e) and Gawad et al. (2007) developed a broadband impedance spectroscopy technique for single-cell analysis in a time window as short as 1 ms. The technique uses a pseudorandom white noise (maximum length sequence, MLS) as a stimulating signal instead of single frequency sinusoidal signals, as shown in Fig. 12a. The MLS single-cell impedance measurement system is shown in Fig. 12b, where the signal generators and lock-in amplifiers of a conventional system (Fig. 9b) are replaced with the MLS signal. Software is used to

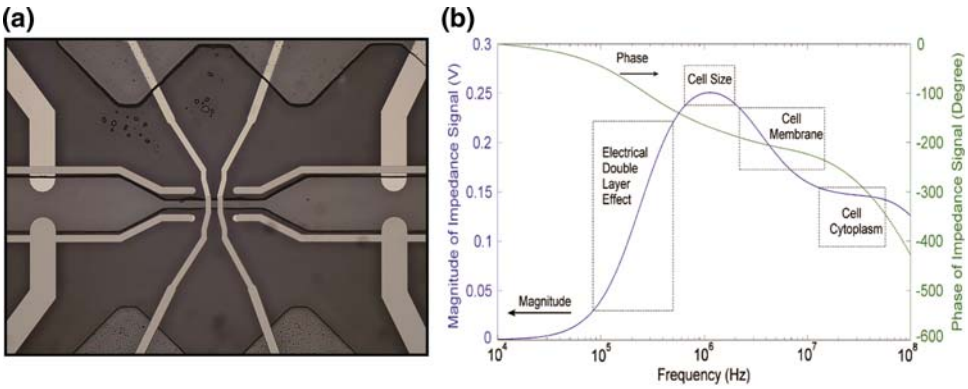

Fig. 11 **a** An example of microfluidic cytometry for single-cell impedance analysis. **b** Plot of the magnitude and phase of the impedance spectra from PSpice circuit simulation

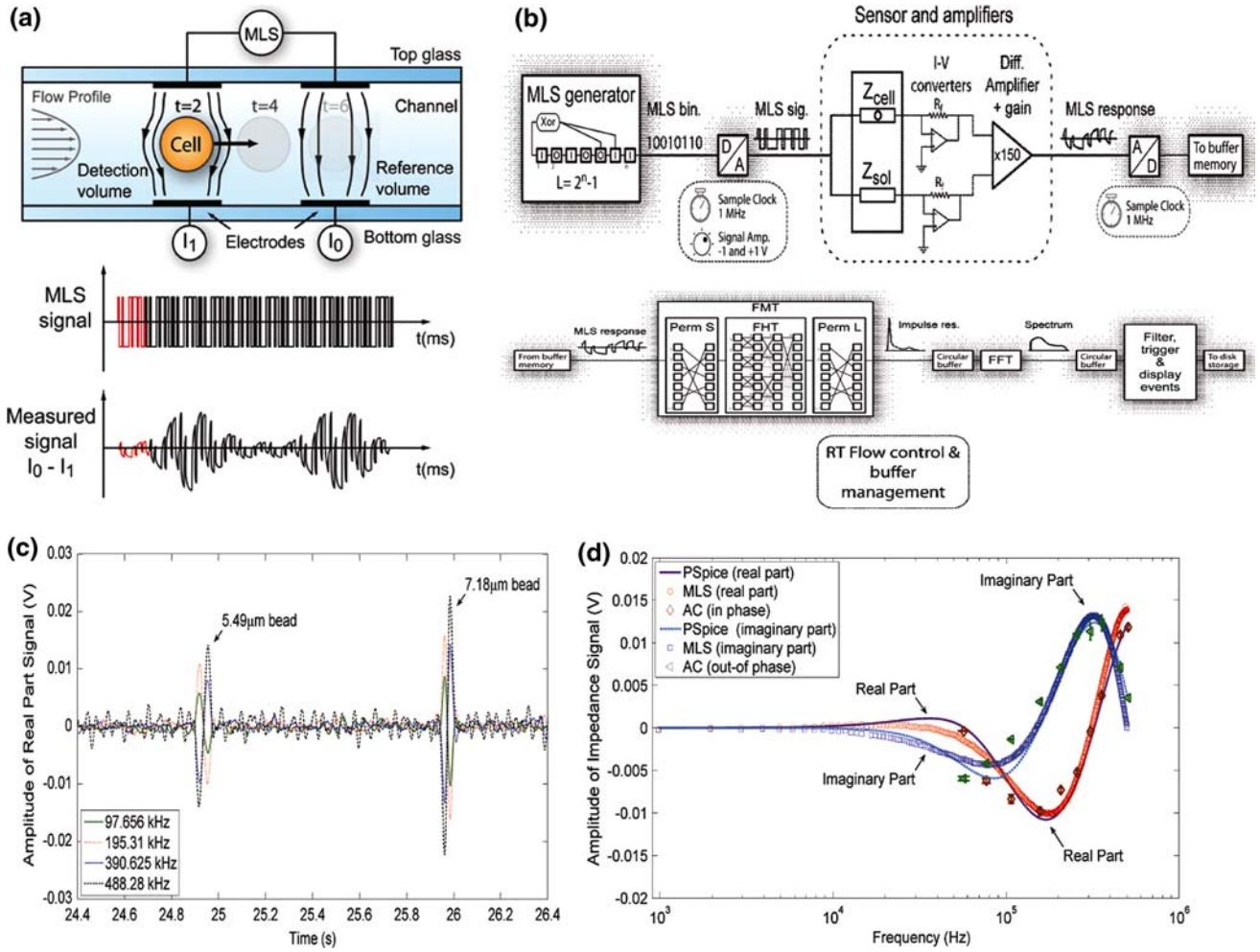

Fig. 12 **a** The principle of MLS single-cell impedance analysis where the electrodes are energised with a pseudo random noise signal which contains all frequencies. **b** The structure and data flow path of the MLS single-cell impedance measurement system (adapted with permission from Gawad et al. 2007, copyright© 2007, AIP). **c** Variations of the real part of the transfer-function signal as a function of time, for two different beads, at four selected frequencies. **d** Real and imaginary parts of the impedance spectrum for the 5.49 μm bead obtained from PSpice simulation, MLS measurements and AC single frequency measurements, showing good agreement (adapted with permission from Sun et al. 2007a, copyright© 2007, RSC)

transform the sampled output response into the impulse response of the system using the Fast M-sequence Transform (FMT). The transfer-function of the system is obtained from Fast Fourier Transform (FFT), finally giving the impedance spectrum. Figure 12c shows variations of the real part of the transfer-function of the system due to the passage of two sizes of beads, plotted for four discrete frequencies (out of 512 separate frequencies measured). The figure demonstrates how MLS measures the impedance of every bead at many different frequencies at the same time. Figure 12d shows the MLS data, the single frequency data and the PSpice simulation results for 5.49 μm diameter beads. MLS measurement provides 512 discrete frequencies in approximately 1 ms. The AC single frequency measurement data for ten different frequencies was measured over several minutes and is the average signal for 200 beads at every frequency. The figure shows good agreement for all three methods, indicating that the MLS system correctly measures the impedance spectrum for a single particle. The upper frequency is limited by the sampling rate of the A/D data acquisition card. However, a limitation of MLS technology is degradation of the SNR of the system, since MLS is extremely vulnerable to slight time variances, for example changes in the flow of cells in the microchannel. Sun et al. (2009b) applied adaptive filtering technique in an adaptive line enhancer mode to reduce the noise.

Taking advantage of laminar flow in microfluidics, hydrodynamic focusing techniques have been used to increase the sensitivity of the system. Rodriguez-Trujillo et al. (2007, 2008) used a sheath flow with a lower conductivity than the sample flow to concentrate the electric

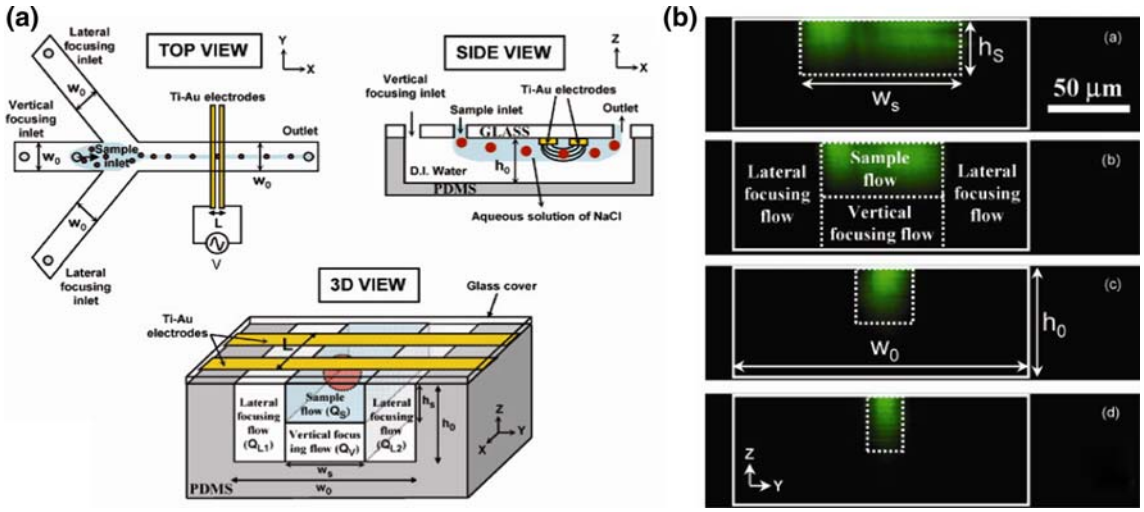

Fig. 13 **a** A micro-device with 2-D hydrodynamic focusing that improves the sensitivity of impedance detection. **b** Confocal images of a cross section of the of the sample solution measurement channel transverse to the direction of flow (adapted with permission from Rodriguez-Trujillo et al. 2008, copyright© 2008, Elsevier)

field lines into the impedance sensing region. As shown in Fig. 13a (Rodriguez-Trujillo et al. 2008), two-dimensional focusing was achieved using an additional orifice drilled in the central inlet channel. The sample is focused into the central stream (in the *y*-direction) and at the same time pushed towards the electrodes (in the *z*-direction), where the electric field strength is high so that the sensitivity is maximised. Since D.I. water (2.1×10^{-4} S/m) is much less conductive than the sample medium (0.15 S/m), the electric field lines are confined within the sample solution, which can be much narrower than the physical geometry of the channel. Figure 13b shows confocal microscopy images of a section transversal to the direction of the fluid in the outlet channel for four different focussing conditions. The sample flux is focused in both lateral and vertical directions to the desired size by adjusting the flowrates of the sheath flows. This technique allows a broad range of particle sizes to be analysed within a single channel. A 2D hydrodynamic focussing scheme was proposed by Scott et al. (2008), in which a stepped outlet channel was fabricated to create a narrow sample stream on the floor of the channel for close interaction with the impedance sensing electrodes. Very recently, a similar focussing strategy to that of Rodriguez-Trujillo et al. (2008) was used by Watkins et al. (2009) to ensure that cells flow in single-file consistently close to the sensing electrodes.

The sensitivity of impedance analysis can be increased further using an insulating sheath flow consisting of an oil phase, focusing a sample into the central stream as shown in Fig. 14a (Bernabini et al. 2010). This figure shows a wide microfluidic channel (250 μm) with pairs of opposing electrodes. The oil sheath ensures that the current density is concentrated only in the conducting liquid. Using this technique, it is possible to detect differences between micron-sized particles in a very wide channel. For example, Fig. 14b and c shows impedance scatter plots for mixtures of beads and *Escherichia coli*. The impedance data are plotted as phase against the magnitude of the low-frequency signal (503 kHz). The data are triggered on the low-frequency in-phase impedance signal and, in both cases, clear discrimination between the two different populations is observed. The volume fraction of the 1 μm diameter particles in this measurement were 0.0036%.

4.2 Impedance analysis of trapped cells

In contrast to continuous flow systems, there is often need to monitor single cells in culture for long periods of time. Microfluidic devices are ideally suited to this, and one example of a multiplexed single-cell assay technology is the hydrodynamic cell trapping arrays, which are used to capture large numbers of individual cells for kinetic analysis within a microfluidic device (Di Carlo et al. 2006a, b). These arrays can be integrated with impedance sensing electrodes, for example, Jang and Wang (2007) fabricated a three-pillar microstructure to capture single-HeLa cells in a microchannel and perform electrical impedance analysis of single cells. Hua and Pennell (2009) fabricated a chevron-like structure of electrodes in a microfluidic channel to capture single cells and measure volume changes using impedance. Malleo et al. (2009) demonstrated continuous differential impedance analysis of single cells held by hydrodynamic cell traps. Figure 15a shows the way in which individually addressable electrodes together with micron-sized traps are integrated in a microfluidic platform. Measurements are performed on cells that are

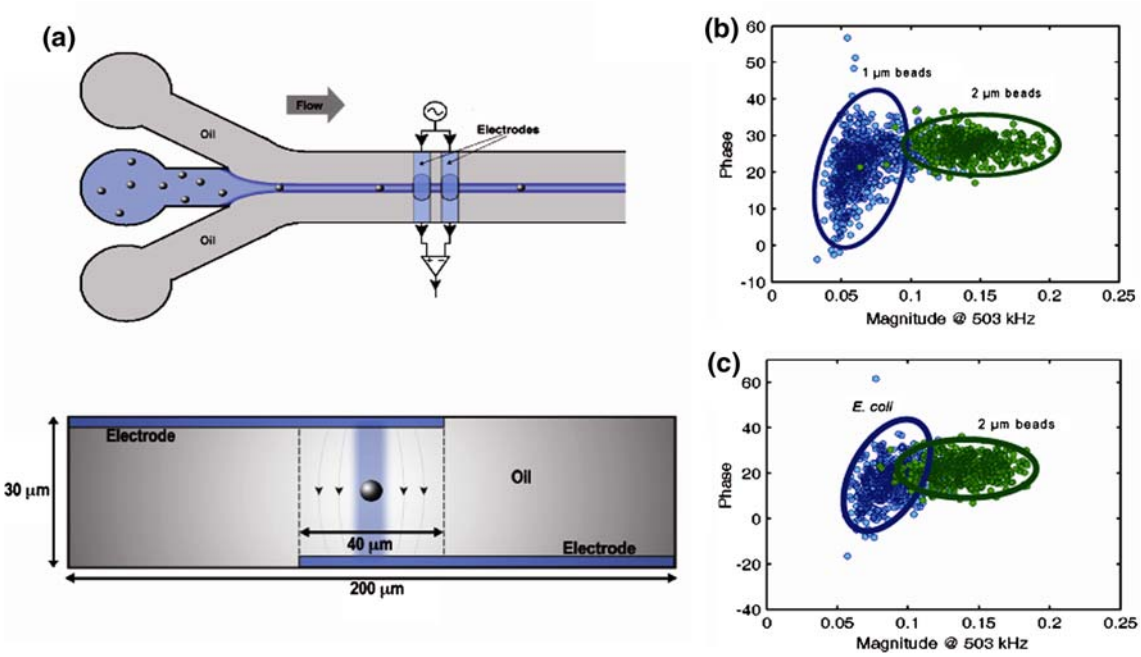

Fig. 14 **a** A hydrodynamic focusing scheme using oil for the sheath flow. **b** Scatter plot of phase against magnitude of the low-frequency impedance for a mixture of 1 and 2 µm diameter polystyrene beads. The plots are colour-coded based on the fluorescence measured from each bead. **c** Scatter plot of phase against low-frequency impedance magnitude for a mixture of *E. coli* and 2-µm diameter polystyrene beads. Plots are colour-coded based on fluorescence

hydrodynamically trapped by normalising the spectrum of a trap containing a single cell to a neighbouring counterpart empty trap. Long-term studies are therefore not influenced by local changes in temperature, pH or conductivity. The system was tested by assaying the transient response of HeLa cells to the lysing effects of the surfactant Tween (Fig. 15b) and the kinetics of the pore-forming toxin streptolysin-O (Fig. 15c) was measured. Perfusion of the toxin elicited exponential decays in the differential impedance response with time constants inversely proportional to toxin concentration. The combination of single hydrodynamic cell trapping with single-cell impedance analysis provides a scalable label-free cell analysis system.

The throughput of cell capturing-type devices is limited unless a large numbers of traps can be fabricated in the channel (Di Carlo et al. 2006a, b; Skelley et al. 2009). The integration of electrodes together with multiplexed impedance measurements increases the complexity of the system compared with flow-through systems and for large arrays of traps complex active matrix methods will be needed to measure the signals from multiple electrodes.

4.3 Applications for clinics and diagnostics

Single-cell impedance analysis methods have recently been developed for biomedical, clinical and point-of-care diagnostic applications. Mishra et al. (2005) used protein-coated microelectrodes to capture the $CD4^+$ cells and showed a linear relationship between the measured impedance and the number of the captured $CD4^+$ cells, although single-cell sensitivity was not demonstrated. The device is aimed at a low cost method for counting $CD4^+$ cells and therefore diagnosing and managing patients with HIV/AIDS. Cheng et al. (2007) used various designs of electrode patterns to count cells by measuring impedance changes in the suspending systems. The detection sensitivity was 20 cells/µl. Single-cell sensitivity was demonstrated by Wang et al. (2008) who integrated a metal oxide semiconductor field effect transistor (MOSFET) into a microfluidic chip, and together with optical detection was able to count purified lymphocytes. The device has the potential to reduce the cost of HIV diagnosis and treatment.

A significant development in the application of single-cell impedance systems was recently demonstrated by Holmes et al. (2009), who showed how a complete (or differential) WBC count could be performed with a few microlitres of human blood. Lymphocytes, monocytes and neutrophils could be separately identified and counted. Figure 16a shows the measured frequency-dependent properties of these three main leukocyte sub-populations, together with PSpice circuit simulations. The data show that the impedance varies with cell size and membrane capacitance across the frequency spectrum. Figure 16b shows an impedance scatter plot for human whole blood (depleted of RBCs), demonstrating that the three common leukocytes can be clearly identified. The microfluidic cytometer was tested

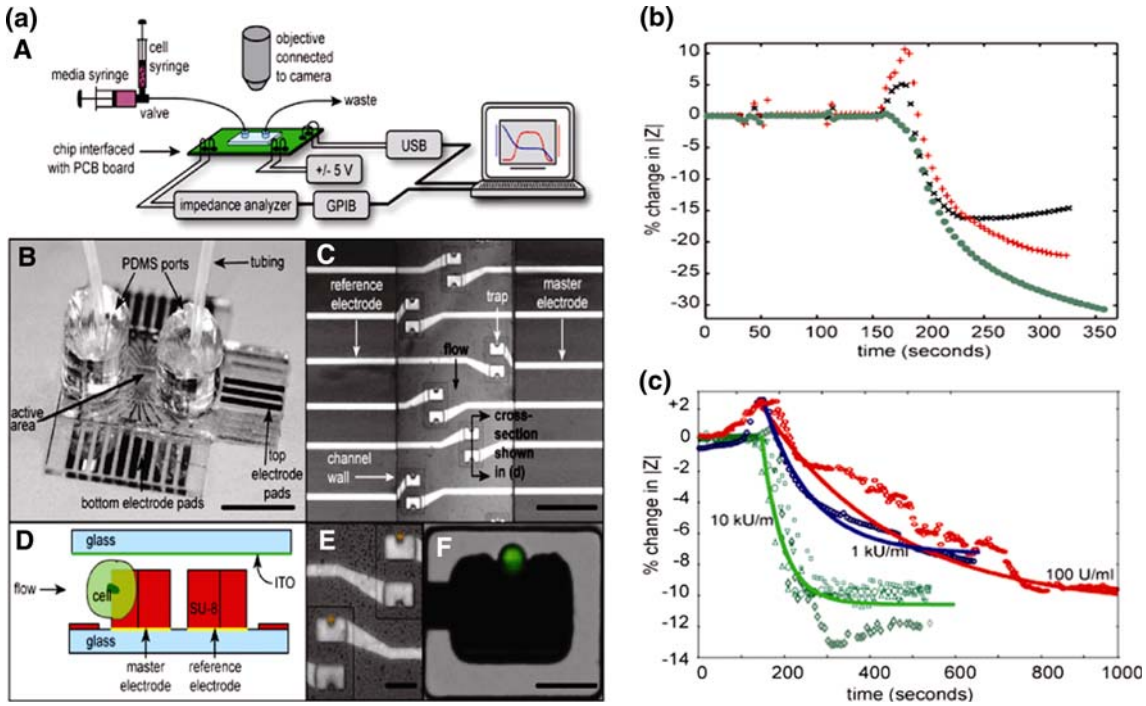

Fig. 15 **a** The experimental system of the cell trap array. The microfluidic device is mounted on a PCB board, which makes electrical connections to the chip and interfaces to a computer and the impedance analyser. **b** Impedance magnitude traces for three individual HeLa cells showing typical changes when a single cell is perfused with Tween 20 causing membrane damage and cell lysis. **c** Data showing the effect of addition of SLO toxin on the impedance spectrum for a single cell. The data were sampled at a frequency of 300 kHz. The exponential curves are the responses for different toxin concentrations, 10, 1 kU/ml, 100 U/ml

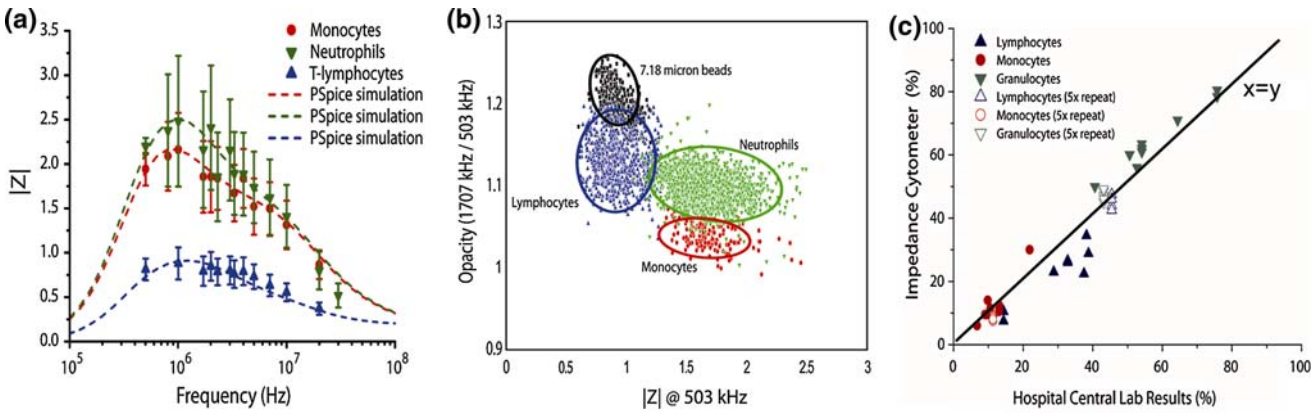

Fig. 16 **a** Frequency spectra of the impedance data for purified sub-populations of T-lymphocytes, monocytes, neutrophils. Each data point comprises approximately 1,500 events and shows the mean and standard deviation of the data. The (*solid*) *dashed lines* show the best fit to the data based on PSPICE circuit simulation of the cell. **b** Scatter plot of opacity versus low-frequency impedance magnitude for saponin/formic acid treated whole human blood, mixed with 7.18 μm beads as a reference sample. **c** Concordance data showing correlation between WBCs counts taken from the micro-impedance cytometer compared those obtained with a commercial blood analyser (adapted with permission from Holmes et al. 2009, copyright© 2009, RSC)

using blood taken from volunteers and benchmarked against a commercial blood analysis system. The lymphocyte, monocyte and granulocyte counts were determined from a 2D Gaussian probability profiles. Figure 16c shows the correlation (95%) between the impedance cytometer and the standard haematology analysis.

5 Conclusions and outlook

The measurement of the passive electrical properties of cell suspensions has a long history. Recent technological developments have now enabled high-speed accurate measurement and characterisation of the electrical

Table 1 Table shows the development of single cell impedance microfluidic cytometry

Authors	Materials Channel (width × height)	Experimental samples	Impedance measurement	Throughput	Summarised results
Larsen et al. (1997)	Etched in silicon Depth: 50 μm	N/A	N/A	N/A	First micro Coulter counter device (no electrical measurements)
Koch et al. (1999)	Etched in silicon Depth: 40 μm	N/A	N/A	N/A	Microfabricated Coulter counter (no results)
Ayliffe et al. (1999)	Epoxy 10 × 4 μm^2	Human PMNs Teleost fish RBCs	Impedance analyser 100 kHz to 2 MHz	N/A	Impedance data at four frequencies for cells (proof to principle)
Fuller et al. (2000)	Photoresist 70 × 20 μm^2	Beads Human peripheral blood granulocytes	Mixed signal electronic circuitry 100 kHz to 10 MHz	N/A	Multi-frequencies impedance measurements of single cells
Sohn et al. (2000)	PDMS 30 × 30/40 μm^2	Eukaryotic cells	Capacitance bridge 1 kHz	N/A	A linear relationship between cell capacitance to size is reported
Saleh and Sohn (2001)	Etched in glass 5.1 × 1.5 × 1 μm^3	Latex particles from 87 to 640 nm	Four-point measurement scheme, DC	3 particles/s	Size measurement of 500 nm colloids with 10 nm resolution
Gawad et al. (2001)	Polyimide 20 × 20 μm^2	5 and 8 μm latex beads Human erythrocytes Erythrocytes ghost cells	Wheatstone bridge 100 kHz to 15 MHz	100 cells/s	First high-throughput single-cell metrology system
Satake et al. (2002)	Etched in silicon Diameter: ~80 μm	Latex particles RBCs	Two-point measurement scheme, DC	N/A	Resistive pulse detection
Saleh and Sohn (2003a)	PDMS Length: 7–9 μm Diameter: 1 μm	Colloids derivatised with streptavidin	Four-point measurement scheme, DC	N/A	Detection of binding of antibodies to the surface of latex colloids
Gawad et al. (2004)	Polyimide 40 × 20 μm^2	4.3 and 5.14 μm latex beads	Trans-impedance 100 kHz to 30 MHz	100 cells/s	Theoretical modelling of single cell impedance
Nieuwenhuis et al. (2004)	Etched in glass Width: 160 μm Depth: 100 μm	25 μm polymer particles	Trans-impedance 50 kHz	N/A	Hydrodynamic focussing defines a 'liquid aperture' for improving sensitivity
Cheung et al. (2005)	Similar to Gawad et al. (2004)	4, 5.14 and 6 μm latex beads RBCs, fixed RBCs, ghosts	Wheatstone bridge 100 kHz to 20 MHz	100 cells/s	Impedance of different sizes of beads and RBCs, ghosts and fixed RBCs
Chun et al. (2005)	Photoresist 50 × 22 μm^2	5.7 and 9.95 μm latex beads Human blood cells	Impedance analyser DC analysis	1000 cells/s	Use of polyelectrolytic salt bridge for counting particles
Wood et al. (2005)	PDMS 50 × 40 μm^2	15 μm beads	Network analyser 10 MHz	25000 beads/s	Radio frequency resonance detection for ultra high-throughput counting
Cho et al. (2006)	Silicon 15 × 4 μm^2	RBCs	Impedance analyser 1 Hz to 10 MHz	N/A	Differentiation of healthy and unhealthy RBCs

Table 1 continued

Authors	Materials Channel (width × height)	Experimental samples	Impedance measurement	Throughput	Summarised results
Morgan et al. (2006, 2007), Benazzi et al. (2007)	Similar to Gawad et al. (2004)	4.5 and 5.5 μm latex beads RBCs Phytoplankton	Differential amplifiers 10 kHz to 10 MHz	100 cells/s	Differentiation of mixed sizes of beads and mixed phytoplanktons
Jagtiani et al. (2006a, b)	Polymer	20 and 40 μm polymethacrylate 20 μm JS pollen and cottonwood pollen particles	Two-point measurement scheme, DC	N/A	A multiple-aperture device
Zhe et al. (2007)	PDMS 100 × 50 μm^2	40 μm PMA particles Juniper pollen	Two-point measurement scheme, DC	N/A	A multiple-channel device
Wood et al. (2007a)	PDMS 100 × 50 μm^2	Barcodes	Network analyser 6.8 MHz	1000 sample/s	Electronic barcode reading technology
Sun et al. (2007d, e), Gawad et al. (2007)	Similar to Gawad et al. (2004)	5.49 and 7.18 μm latex beads RBCs	Trans-impedance 1–500 kHz	100 cells/s	Multi-frequency impedance analysis of single cells in a short time period using MLSs
Jang and Wang (2007)	PDMS 100 × 25 μm^2	HeLa cell	Impedance analyser 1–100 kHz	N/A	Single HeLa cell is captured and measured using impedance
Rodriguez-Trujillo et al. (2007, 2008)	PDMS 190 × 50 μm^2 or similar	20 μm beads	Impedance analyser 120 kHz and 1 MHz	20 beads/s	Hydrodynamic focalisation is used to improve sensitivity
Küttel et al. (2007)	Similar to Gawad et al. (2001)	Babesia bovis infected RBCs	Lock-in amplifiers at 8.7 MHz	N/A	Impedance detection of parasitised cell population
Wang et al. (2008)	PDMS 16 × 30 μm^2	CD4+ T cells	MOSFET drain current detection	8 cells/s	Passage of single cells recorded by monitoring variation in MOSFET drain current
Wu et al. (2008a)	PDMS 50 × 16 × 20 μm^3	520 nm, 1, 2 and 4.84 μm beads	Differential amplifier	N/A	Detection of a minimum volume fraction of 0.0004%
Scott et al. (2008)	PDMS 100 × 90μm^2	20 μm beads	Lock-in amplifier 30–50 kHz	50 beads/s	A 3D hydrodynamic focussing scheme
Zheng et al. (2008)	Parylene PDMS	5, 8 and 10 μm latex beads RBCs	Impedance analyser 100 Hz to 7 MHz	N/A	Platinum-black electrodes to reduce the EDL effect
Hua and Pennell (2009)	SU8 125 × 17 μm^2	Madin-Darby Canine Kidney (MDCK) epithelial cells	Differential amplifiers 50 Hz	N/A	Single MDCK cell is captured and impedance data to osmotic changes
Malleo et al. (2009)	SU8 Height: 29 μm	HeLa cell	Impedance analyser 100 Hz and 2 MHz	N/A	Differential captured single-cell impedance measurements
Watkins et al. (2009)	PDMS 200 × 32 μm^2	CD4+ T-lymphocytes	Lock-in amplifiers 50 kHz	N/A	A 3-D hydrodynamic focussing scheme
Holmes et al. (2009)	Similar to Gawad et al. (2004)	Whole blood	Differential amplifier 500 kHz to 30 MHz	100 cells/s	Three-part differentiation of leukocytes: T-lymphocytes, monocytes and neutrophils in human blood

properties of single cells. Many research groups are developing variants of the Coulter technology, which provides limited but nevertheless useful information on cell numbers and size. A wide range of different approaches have been used to the measurement of single cell and a summary of the papers and technologies is listed in Table 1. The earliest reports in 1997 and 1999 demonstrated the principle of a micro-fabricated Coulter counter, although no electrical data on particles were presented.

The Coulter approach still dominates the field, primarily because these devices are relatively easy to fabricate. Detection techniques vary from simple low-frequency AC bridge circuits, commercial impedance analysers or RF resonance methods capable of very high-speed single particle counting. The throughput of the devices is up to 100 s of cells per second, still much lower than optical flow cytometry. However, improvement in technology and electronics will allow single-cell impedance cytometry to compete with conventional flow cytometry and achieve high throughputs. Multi-frequency impedance analysis provides much more information, including data on the characteristics of the cell membrane and cytoplasm. As discussed in this review, details of the cell membrane capacitance (together with cell size) can be used to discriminate between different blood leukocytes. High-frequency measurements of the cytoplasm can provide information about the internal composition of cells and for example whether cells are invaded by parasites.

The technology should find applications in a number of diagnostic and research areas for example cell cycle analysis, measurement of apoptosis and toxicity/viability assays. For example, experiments have shown differences in the electrical properties of lymphocytes and other cells exposed to various stimuli such as bacterial or viral products or mitogens, e.g. lipopolysaccharides. In general, the measured changes in membrane capacitance are accounted for differences in cell membrane structure caused by features such as micro-villi, folds and blebs account Huang et al. (1999) showed that mitogenic stimulation of human T-lymphocytes, using phytohemagglutinin (PHA) and interleukin-2 (IL-2), caused changes in the membrane dielectric properties that correlated with phase of the cell cycle. They showed that the membrane capacitance of cells increased by 30%, 48 h after stimulation. Wang et al. (2002) showed changes in the dielectric properties of HL-60 and Jurkat cells during apoptosis. In the HL-60 cells, the membrane capacitance fell by nearly 50% 4 h after treatment. There were significant changes in the membrane capacitance as early as 1 h after treatment. A range of other single-cell processes could also be probed by impedance spectroscopy, such as the effect of toxicants (Ratanachoo et al. 2002) and virus (Archer et al. 1999).

Although impedance measurements are label-free and can provide information on cell phenotype, they can never match the sensitivity and specificity afforded by the fluorescent antibody labelling techniques used in commercial flow cytometry. The wide spectral bandwidth available using optical techniques means that many different cell subtypes can be simultaneously analysed and identified. Electrical impedance cannot detect different antigen expressing cell sub-types with similar morphology. However, a method analogous to fluorescent antibody labelling has recently been demonstrated which allows the discrimination of antigenically specific WBCs (Holmes and Morgan 2010). This has been demonstrated through the impedance identification of lymphocyte sub-set, expressing the CD4 surface protein. A suspension of WBCs was complexed with micron-sized polymer beads that had been coated in an antibody that specifically recognises the CD4 antigen. The beads bind to the CD4 expressing cells (and to a lesser extent the monocytes; the populations can be easily discriminated from due to their larger size of the later) and in doing so change the impedance properties of these cells. This experiment demonstrates that it is possible to use "electrical labels" to selectively alter the impedance properties of certain cell sub-populations, and provides a route to the use of labels for further discrimination of cells. Although this is a promising method for identifying cells expressing one unique antigen marker, impedance measurements cannot provide the wide spectrum offered by optical fluorescent labels. High-throughput microfluidic single-cell impedance metrology is an important area that will continue to develop. This will be facilitated by technologies that enable faster sampling and extension of the frequency window, both at the low and high ends. Further innovations are required; including novel methods that enable further differentiation of subtle changes in cell morphology that could lead to further non-invasive analysis of cell parameters, including cell cycle and apoptotic events.

Acknowledgements We acknowledge EPSRC/TSB for funding (Technology Program TS/G001405) and Dr. David Holmes for discussions. T. Sun would like to acknowledge the postdoctoral fellowship from National Centre for the Replacement, Refinement and Reduction of Animals in Research (NC3Rs), UK.

References

Archer S, Morgan H, Rixon FJ (1999) Electrorotation studies of baby hamster kidney fibroblasts infected with herpes simplex virus type 1. Biophys J 76:2833–2842

Arnold WM, Zimmermann U (1988) Electro-rotation: development of a technique for dielectric measurements on individual cells and particles. J Electrostat 21:151–191

Asami K (2002) Characterization of heterogeneous systems by dielectric spectroscopy. Prog Polym Sci 27:1617–1659

Asami K (2006) Dielectric dispersion in biological cells of complex geometry simulated by the three-dimensional finite difference method. J Phys D Appl Phys 39:492–499

Ayliffe HE, Frazier AB, Rabbit RD (1999) Electric impedance spectroscopy using microchannels with integrated metal electrodes. J Microelectromech Syst 8:50–57

Bard AJ, Faulkner LR (2000) Electrochemical methods: fundamentals and applications, 2nd edn. Wiley, New York

Bayley H, Martin CR (2000) Resistive-pulse sensing—from microbes to molecules. Chem Rev 100:2575–2594

Beebe DJ, Mensing GA, Walker GM (2002) Physics and applications of microfluidics in biology. Annu Rev Biomed Eng 4: 261–286

Benazzi G, Holmes D, Sun T, Mowlem M, Morgan H (2007) Discrimination and analysis of phytoplankton using a microfluidic cytometer. IET Nanobiotechnol 1:94–101

Bernabini C, Holmes D, Morgan H (2010) Detection and discrimination of bacteria and micro-particles by micro-impedance spectroscopy. Lab Chip (submitted)

Branton D et al (2008) The potential and challenges of nanopore sequencing. Nat Biotechnol 26:1146–1153

Brown RB, Audet J (2008) Current techniques for single cell analysis. J R Soc Interface 5:S131–S138

Bruggeman DAG (1935) Berechnug vershiedener physikalischen Konstanten von heterogenen substanzen. Ann Phys (Leipzig) 24:634–636

Carlo DD, Wu LY, Lee LP (2006a) Dynamic single cell culture array. Lab Chip 6:1445–1449

Carlo DD, Wu LY, Lee LP (2006b) Single-cell enzyme concentrations, kinetics, and inhibition analysis using high-density hydrodynamic cell isolation arrays. Anal Chem 78:4925–4930

Chao TC, Ros A (2008) Microfluidic single-cell analysis of intracellular compounds. J R Soc Interface 5:S139–S150

Cheng X, Liu Y, Irimia D, Demirci U, Yang L, Zamir L, Toner M, Rodríguez, Bashir R (2007) Cell detection and counting through cell lysate impedance spectroscopy in microfluidic devices. Lab Chip 7:746–755

Cheung K, Gawad S, Renaud Ph (2005) Impedance spectroscopy flow cytometry: on-chip label-free cell differentiation. Cytometry A 65A:124–132

Cho YH, Yamamoto T, Sakai Y, Fujii T, Kim B (2006) Development of microfluidic device for electrical/physical characterization of single cell. J Microelectromech Syst 15:287–295

Chun H, Chung TD, Kim HC (2005) Cytometry and velocimetry on a microfluidic chip using poly electrolytic salt bridges. Anal Chem 77:2490–2495

Cole KS (1928a) Electric impedance of suspensions of spheres. J Gen Physiol 12:29–36

Cole KS (1928b) Electric impedance of suspensions of Arbacia eggs. J Gen Physiol 12:37–54

Cole KS (1932) Electric phase angle of cell membranes. J Gen Physiol 15:641–649

Cole KS (1935) Electric impedance of Hipponoë eggs. J Gen Physiol 18:877–887

Cole KS, Cole RH (1936a) Electric impedance of Asteria eggs. J Gen Physiol 19:609–623

Cole KS, Cole RH (1936b) Electric impedance of Arbacia eggs. J Gen Physiol 19:625–632

Coulter WH (1956) High speed automatic blood cell counter and cell analyzer. Proc Natl Electron Conf 12:1034–1040

Curtis HJ, Cole KS (1937) Transverse electric impedance of Nitella. J Gen Physiol 21:189–201

Davey HM, Kell DB (1996) Flow cytometry and cell sorting of heterogeneous microbial populations: the importance of single-cell analyses. Microbiol Rev 60:641–696

Deblois RW, Bean CP (1970) Counting and sizing of submicron particles by the resistive pulse technique. Rev Sci Instrum 41:909–916

Ferrier GA, Romanuik SF, Thomson DJ, Bridges GE, Freeman MR (2009) A microwave interferometric system for simultaneous actuation and detection of single biological cells. Lab Chip 9:3406–3412

Foster KR (2002) Herman P. Schwan: a scientist and pioneer in biomedical engineering. Annu Rev Biomed Eng 4:1–27

Foster KR, Schwan HP (1989) Dielectric properties of tissues and biological materials: a critical review. Crit Rev Biomed Eng 17:25–104

Fricke H (1924a) A mathematical treatment of the electrical conductivity of colloids and cell suspensions. J Gen Physiol 6:375–384

Fricke H (1924b) A mathematical treatment of the electric conductivity and capacity of disperse systems. I. The electric conductivity of a suspension of homogeneous spheroids. Phys Rev 24:575–587

Fricke H (1925a) A mathematical treatment of the electric conductivity and capacity of disperse systems. II. The capacity of a suspension of conducting membrane for a current of low frequency. Phys Rev 26:678–681

Fricke H (1925b) The electric capacity of suspensions of a red corpuscles of a dog. Phys Rev 26:682–687

Fricke H (1925c) The electric capacity of suspensions with special reference to blood. J Gen Physiol 9:137–152

Fricke H (1925d) The electric resistance and capacity of blood for frequencies between 800 and 4.5 million cycles. J Gen Physiol 9:153–167

Fuller CK, Hamilton J, Ackler H, Krulevitch P, Boser B, Eldredge A, Becker F, Yang J, Gascoyne P (2000) Microfabricated multi-frequency particle impedance characterization system. In: Proceedings of the μTAS symposium, Enschede, The Netherlands, May 2000, pp 265–268

Gawad S, Schild L, Renaud Ph (2001) Micromachined impedance spectroscopy flow cytometer for cell analysis and particle sizing. Lab Chip 1:76–82

Gawad S, Cheung K, Seger U, Bertsch A, Renaud Ph (2004) Dielectric spectroscopy in a micromachined flow cytometer: theoretical and practical considerations. Lab Chip 4:241–251

Gawad S, Sun T, Green NG, Morgan H (2007) Impedance spectroscopy using maximum length sequences: application to single cell analysis. Rev Sci Instrum 78:054301

Hanai T (1960) Theory of the dielectric dispersion due to the interfacial polarization and its application to emulsion. Kolloid Z 171:23–31

Hanai T, Koizumi N (1976) Numerical estimation on a theory of interfacial polarization developed for disperse systems in higher concentration. Bull Inst Chem Res Kyoto Univ 54:248–254

Hanai T, Koizumi N, Irimajiri A (1975) A method for determining the dielectric constant and the conductivity of membrane-bounded particles of biological relevance, Biophys. Struct Mech 1:285–294

Hanai T, Asami K, Koizumi N (1979) Dielectric theory of concentrated suspensions of shell-spheres in particular reference to the analysis of biological cell suspensions. Bull Inst Chem Res Kyoto Univ 57:297–305

Höber R (1910) Eine Methode die elektrische Leitfaehigkeit im Innern von Zellenzu messen. Arch Ges Physiol 133:237–259

Höber R (1912) Ein zweites Verfahren die Leitfaehigkeit im Innern von Zellen ze messem. Arch Ges Physiol 148:189–221

Höber R (1913) Messungen der inneren Leitfaehigkeit von Zelen III. Arch Ges Physiol 150:15–45

Hoffman RA, Britt WB (1979) Flow-system measurement of cell impedance properties. J Histochem Cytochem 27:234–240

Hoffman RA, Johnson TS, Britt WB (1981) Flow cytometric electronic direct current volume and radiofrequency impedance measurements of single cells and particles. Cytometry 1: 377–384

Holmes D, Morgan H (2010) Single cell impedance cytometry for identification and counting of CD4 T-cells in human blood using impedance labels. Anal Chem 82:1455–1461

Holmes D, Pettigrew D, Reccius CH, Gwyer JD, Berkel CV, Holloway J, Davie DE, Morgan H (2009) Leukocyte analysis and differentiation using high speed microfluidic single cell impedance cytometry. Lab Chip 9:2881–2889

Hua SZ, Pennell (2009) A microfluidic chip for real-time studies of the volume of single cells. Lab Chip 9:251–256

Huang Y, Wang XB, Tame JA, Pethig R (1993) Electrokinetic behaviour of colloidal particles in travelling electric-fields: studies using yeast cells. J Phys D Appl Phys 26:1528–1535

Huang Y, Wang XB, Gascoyne PRC, Becker FF (1999) Membrane dielectric responses of human T-lymphocytes following mitogenic stimulation. Biochimica Biophys Acta 1417:51–62

Iliescu C, Poenar DP, Carp M, Loe FC (2007) A microfluidic device for impedance spectroscopy analysis of biological samples. Sens Actuators B 123:168–176

Jagtiani AV, Zhe J, Hu J, Carletta J (2006a) Detection and counting of micro-scale particles and pollen using a multi-aperture Coulter counter. Meas Sci Technol 17:1706–1714

Jagtiani AV, Sawant R, Zhe J (2006b) A label-free high throughput resistive-pulse sensor for simultaneous differentiation and measurement of multiple particle-laden analytes. J Micromech Microeng 16:1530–1539

Jang LS, Wang MH (2007) Microfluidic device for cell capture and impedance measurement. Biomed Microdevices 9:737–743

Jones TB (1995) Electromechanics of particles. Cambridge University Press, Cambridge, UK

Kampmann GS, Huwiler A, Hebeisen M, Hessler T, Berardino MD (2008) On-chip non-invasive and label-free cell discrimination by impedance spectroscopy. Cell Prolif 41:830–840

Kim KB, Chun H, Kim HC, Chung TD (2009) Red blood cell quantification microfluidic chip using polyelectrolytic gel electrodes. Electrophoresis 30:1464–1469

Koch M, Evans AGR, Brunnschweller A (1999) Design and fabrication of a micromachined Coulter counter. J Micromech Microeng 9:159–161

Küttel C, Nascimento E, Demierre N, Silva T, Braschler T, Renaud Ph, Oliva AG (2007) Label-free detection of *Babesia bovis* infected red blood cells using impedance spectroscopy on a microfabricated flow cytometer. Acta Trop 102:63–68

Larsen U, Blankenstein G, Branebjerg J (1997), Microchip Coulter particle counter. In: Technical digest of the international conference on solid-state sensors and actuators, Chicago, IL, pp 1319–1322

Linderholm P, Renaud Ph (2005) Comment on 'AC frequency characteristics of coplanar impedance sensors as design parameters'. Lab Chip 5:270–279

Linderholm P, Seger U, Renaud Ph (2006) Analytical expression for electric field between two facing strip electrodes in microchannel. Electron Lett IEE 42:145–147

Lu H, Schmidt MA, Jensen KF (2005) A microfluidic electroporation device for cell lysis. Lab Chip 5:23–29

Malleo D, Nevill JT, Lee LP, Morgan H (2009) Continuous differential impedance spectroscopy of single cells. Microfluid Nanofluid. doi:10.1007/s10404-009-0534-2

Manz A, Harrison DJ, Verpoorte EMJ, Fettinger JC, Paulus A, Lüdi H, Widmer HM (1992) Planar chips technology for miniaturization and integration of separation techniques into monitoring systems-capillary electrophoresis on a chip. J Chromatog 593:253–258

Maxwell JC (1873) A treatise on electricity and magnetism. Clarendon Press, Oxford

Mishra NN, Retterer S, Zieziulewicz TJ et al (2005) On-chip microbiosensor for the detection of human CD4(+) cells based on AC impedance and optical analysis. Biosens Bioelectron 21:696–704

Morgan H, Green NG (2003) AC electrokinetics: colloids and nanoparticles. Research Studies Press, Ltd., Baldock

Morgan H, Green NG, Hughes MP, Monaghan W, Tan TC (1997) Large area travelling-wave dielectrophoresis particle separator. J Micromech Microeng 7:65–70

Morgan H, Holmes D, Green NG (2006) High speed simultaneous single particle impedance and fluorescence analysis on a chip. Curr Appl Phys 6:367–370

Morgan H, Sun T, Holmes D, Gawad S, Green NG (2007) Single cell dielectric spectroscopy. J Phys D Appl Phys 40:61–70

Murali S, Jagtiani AV, Xia X, Carletta J, Zhe J (2009) A microfluidic Coulter counting device for metal wear detection in lubrication oil. Rev Sci Instrum 80:016105

Nieuwenhuis JH, Kohl F, Bastemeijer J, Sarro PM, Vellekoop MJ (2004) Integrated Coulter counter based on 2-dimensional liquid aperture control. Sens Actuators B 102:44–50

Pauly H, Schwan HP (1959) Uber die Impedanz einer Suspension von kugelformigen Teilchen mit einer Schale. Z Naturf B 14:125–131

Pethig R (1979) Dielectric and electronic properties of biological materials. Wiley, Chichester, UK

Pohl HA (1978) Dielectrophoresis. Cambridge University Press, Cambridge, UK

Ratanachoo K, Gascoyne PRC, Ruchirawat M (2002) Detection of cellular response to toxicants by dielectrophoresis. Biochimica Biophysica Acta 1564:449–458

Rodriguez-Trujillo R, Mills CA, Samitier J, Gomila G (2007) Low cost micro-Coulter counter with hydrodynamic focusing. Microfluid Nanofluid 3:171–176

Rodriguez-Trujillo R, Castillo-Fernandez O, Garrido M, Arundell M, Valencia A, Gomila G (2008) High-speed particle detection in a micro-Coulter counter with two-dimensional adjustable aperture. Biosens Bioelectron 24:290–296

Saleh OA, Sohn LL (2001) Quantitative sensing of nanoscale colloids using a microchip Coulter counter. Rev Sci Instrum 72:4449–4451

Saleh OA, Sohn LL (2003a) Direct detection of antibody-antigen binding using an on-chip artificial pore. PNAS 100:820–824

Saleh OA, Sohn LL (2003b) An artificial nanopore for molecular sensing. Nano Lett 3:37–38

Satake D, Ebi H, Oku N, Matsuda K, Takao H, Ashiki M, Ishida M (2002) A sensor for blood cell counter using MEMS technology. Sens Actuators B 83:77–81

Schwan HP (1957) Electrical properties of tissue and cell suspensions. Adv Biol Med Phys 5:147–209

Schwan HP (1963) Determination of biological impedances. In: Nastuk WL (ed) Physical techniques in biological research, vol 6. Academic Press, New York, pp 323–406

Schwan HP (1968) Electrode polarization impedance and measurements in biological materials. Ann N Y Acad Sci 148:191–209

Scott R, Sethu P, Harnett CK (2008) Three-dimensional hydrodynamic focusing in a microfluidic Coulter counter. Rev Sci Instrum 79:046104

Shapiro HM (2004) The evolution of cytometers. Cytometry A 58A:13–20

Shuler ML, Aris R, Tsuchiya HM (1972) Hydrodynamic focusing and electronic cell-sizing techniques. Appl Microbiol 24:384–388

Sims CE, Allbritton NL (2007) Analysis of single mammalian cells on-chip. Lab Chip 7:423–440

Skelley AM, Kirak O, Suh H, Jaenisch R, Voldman J (2009) Microfluidic control of cell pairing and fusion. Nat Methods 6:147–152

Sohn LL, Saleh OA, Facer GR, Beavis AJ, Allan RS, Notterman DA (2000) Capacitance cytometry: measuring biological cells one by one. PNAS 97:10687–10690

Spielman L, Gorsen SL (1968) Improving resolution in Coulter counting by hydrodynamic focusing. J Colloid Interface Sci 26:175–182

Squires TM, Quake SR (2005) Microfluidics: fluidic physics at the nanoliter scale. Rev Mod Phys 77:977–1026

Stewart DA, Gowrishankar TR, Smith KC, Weaver JC (2005) Cylindrical cell membranes in uniform applied electric field: validation of a transport lattice method. IEEE Trans Biomed Eng 52:1643–1653

Stone HA, Stroock AD, Ajdari A (2004) Engineering flows in small devices: microfluidics toward a lab-on-a-chip. Annu Rev Fluid Mech 36:381–411

Sun T, Morgan H, Green NG (2007a) Analytical solutions of ac electrokinetics in interdigitated electrode arrays: electric field, dielectrophoretic and travelling-wave dielectrophoretic forces. Phys Rev E 76:046610

Sun T, Gawad S, Green NG, Morgan H (2007b) Dielectric spectroscopy of single cells: time domain analysis using Maxwell's mixture equation. J Phys D Appl Phys 40:1–8

Sun T, Green NG, Gawad S, Morgan H (2007c) Analytical electric field and sensitivity analysis for two microfluidic impedance cytometer designs. IET Nanobiotechnol 1:69–79

Sun T, Gawad S, Bernabini C, Green NG, Morgan H (2007d) Broadband single cell impedance spectroscopy using maximum length sequences: theoretical analysis and practical considerations. Meas Sci Technol 18:2859–2868

Sun T, Holmes D, Gawad S, Green NG, Morgan H (2007e) High speed multi-frequency impedance analysis of single particles in a microfluidic cytometer using maximum length sequences. Lab Chip 7:1034–1040

Sun T, Bernabini C, Morgan H (2009a) Single-colloidal particle impedance spectroscopy: complete equivalent circuit analysis of polyelectrolyte microcapsules. Langmuir. doi:10.1021/1a903609u

Sun T, Berkel CV, Green NG, Morgan H (2009b) Digital signal processing methods for impedance microfluidic cytometry. Microfluid Nanofluid 6:179–187

Svahn HA, Berg AVD (2007) Single cells or large populations. Lab Chip 7:544–546

Tang H, Gao Y (2005) An impedance microsensor with coplanar electrodes and vertical sensing apertures. IEEE Sens 5:1346–1352

Thorsen T, Maerkl SJ, Quake SR (2002) Microfluidic large-scale integration. Science 298:580–584

Tsong TY (1991) Electroporation of cell membranes. Biophys J 60:297–306

Voldman J (2006) Electrical forces for microscale cell manipulation. Annu Rev Biomed Eng 8:425–454

Wachner D, Simeonova M, Gimsa J (2002) Estimating the subcelluar absorption of electric field energy: equations for an ellipsoidal single shell model. Bioelectrochemistry 56:211–213

Wang XB, Huang Y, Holzel R, Burt JPH, Pethig R (1993) Theoretical and experimental investigations of the interdependence of the dielectric, dielectrophoretic and electrorotational behaviour of colloidal particles. J Phya D Appl Phys 26:312–322

Wang X, Becker FF, Gascoyne PRC (2002) Membrane dielectric changes inside induced apoptosis in HL-60 cells more sensitively than surface phosphatidylserine expression or DNA fragmentation. Biochimica Biophysica Acta 1564:412–420

Wang Y-N, Kang Y, Xu D, Chon CH, Barnett L, Kalams SA, Li D, Li D (2008) On-chip counting the number and the percentage of CD4+ T lymphocyte. Lab Chip 8:309–315

Watkins N, Venkatesan BM, Toner M, Rodriguez W, Rashid B (2009) A robust electrical microcytometer with 3-dimensional hydrofocusing. Lab Chip 9:3177–3184

Whitesides GM (2006) The origins and the future of microfluidics. Nature 442:368–373

Whitesides GM, Stroock AD (2001) Flexible methods for microfluidics. Phys Today 54:42–48

Wood DK, Oh SH, Lee SH, Soh HT, Cleland AN (2005) High-bandwidth radio frequency Coulter counter. Appl Phys Lett 87:184106

Wood DK, Braun GB, Fraikin JL, Swenson LJ, Reich NO, Cleland AN (2007a) A feasible approach to all-electronic digital labelling and readout for cell identification. Lab Chip 7:469–474

Wood DK, Requa MV, Cleland AN (2007b) Microfabricated high-throughput electronic particle detector. Rev Sci Instrum 78:104301

Wu X, Kang Y, Wang Y-N, Xu D, Li D, Li D (2008a) Microfluidic differential resistive pulse sensors. Electrophoresis 29:2754–2759

Wu X, Chon CH, Wang Y-N, Kang Y, Li D (2008b) Simultaneous particle counting and detecting on a chip. Lab Chip 8:1943–1949

Yang J, Huang Y, Wang XJ, Becker FF, Gascoyne PRC (1999) Dielectric properties of human leukocyte subpopulations determined by electrorotation as a cell separation criterion. J Biophys 76:3307–3314

Zhang H, Chon CH, Pan X, Li D (2009) Methods for counting particles in microfluidic applications. Microfluid Nanofluid 7:739–749

Zhe J, Jagtiani A, Dutta P, Hu J, Carletta J (2007) A micromachined high throughput Coulter counter for bioparticle detection and counting. J Micromech Microeng 17:303–313

Zheng S, Liu M, Tai Y-C (2008) Micro coulter counters with platinum black electropolated electrodes for human blood cell sensing. Biomed Microdevices 10:221–231